

A physically based distributed karst hydrological model (QMG model-V1.0) for flood ~~simulation~~simulation

Ji Li^{1,*}, Daoxian Yuan^{1,2}, Fuxi-Zhang³, Jiao Liu⁴, Mingguo Ma¹

¹Chongqing Jinpo Mountain Karst Ecosystem National Observation and Research Station, Chongqing Key Laboratory of Karst Environment, School of Geographical Sciences, Southwest University, Chongqing 400715, China

²Key Laboratory of Karst Dynamics, MNR & Guangxi, Institute of Karst Geology, Chinese Academy of Geological Sciences, Guilin 541004, China

³College of Engineering Science and Technology, Shanghai Ocean University; Shanghai Engineering Research Center of Marine Renewable Energy 201306, China

⁴Chongqing municipal hydrological monitoring station, Chongqing 401120, China

Corresponding author: Ji Li (445776649@qq.com)

Abstract Karst trough ~~valleys~~and valley landforms are prone to flooding, primarily because of the unique hydrogeological features of karst ~~landform~~landforms, which are conducive to the spread of rapid runoff. Hydrological models that represent the complicated hydrological processes in karst regions are effective for predicting karst flooding, but their application has been hampered by their complex model structures and associated parameter ~~set~~sets, especially ~~so~~ for distributed hydrological models, which require large amounts of hydrogeological data. Distributed hydrological models for predicting ~~the Karst~~ flooding ~~is~~are highly dependent on distributed ~~structures~~modeling~~modelling~~ processes, complicated boundary ~~parameters~~setting~~parameter~~ settings, and ~~tremendous~~extensive hydrogeological data processing ~~that is both~~steps, which are time ~~and computational power~~ consuming.

~~Proposed here is~~ and computationally expensive. In this study, a distributed physically-based karst hydrological model, ~~known as~~ called the QMG (Qingmuguan) model is proposed. The structural design of this model is relatively simple, and it is generally divided into surface and underground double-layered structures. The parameters that represent the structural functions of each layer have clear physical meanings, and ~~the fewer~~ fewer parameters are ~~less required~~ than those of the current are need for other distributed models. This approach allows ~~modeling in~~ karst areas to be modelled with only a small amount of necessary hydrogeological data. ~~18~~Eighteen flood processes ~~aeross~~associated with the karst underground river in the Qingmuguan karst trough valley are simulated by the QMG model, and the simulated values agree well with observations, for which the average value of the Nash–Sutcliffe coefficient ~~was~~is 0.92. A sensitivity analysis shows that the infiltration coefficient, permeability coefficient, and rock porosity are the most important parameters ~~that require the most attention~~ in model calibration and optimization. The improved ~~predictability~~predictions of karst flooding ~~by~~obtained with the proposed QMG model ~~promotes a better~~ enhance the mechanistic ~~depicting~~understanding of runoff generation and ~~confluence~~flow in karst trough valleys.

Keywords: Simulation and forecasting of karst floods; Karst trough valleys; QMG (Qingmuguan) model; Parametric optimization; Parameter sensitivity analysis

1 Introduction

Karst trough ~~valleys and~~ valley landforms are very common in China, especially in the southwest. In general, these karst areas are water scarce during most of the year because their surfaces store very little rainfall, but they are also potential ~~birthplaces for~~sources of floods because the local trough and valley landforms and topographic features facilitate the

formation and propagation of floods ([White, 2002](#); Li et al., 2021). ~~Taking the~~The coexistence of drought and flood is a typical phenomenon in these karst trough and valley areas. For example ~~of, in~~ the present study area, ~~i.e.~~ the Qingmuguan karst trough valley, floods ~~used to happen here constantly~~were historically prevalent during the rainy season. In recent years, with more extreme rainfall events and the increased area of construction land in the region, rainfall infiltration has decreased, and rapid runoff over impervious surfaces has increased, resulting in frequent catastrophic flooding in the basin (Liu et al., 2009). Excess water ~~overflows~~flows from karst sinkholes and underground river outlets ~~often occur~~ during floods; ([Jourde et al., 2007, 2014](#); [Martinotti et al., 2017](#)), flooding large areas of farmland and residential areas and causing serious economic losses ([Gutierrez, 2010](#); [Parise, 2010](#); Yu et al., 2020). Therefore, it is both important and urgent to simulate and predict karst flooding events in karst trough ~~valleys~~and valley regions, such as the study area.

Hydrological models can be effective for forecasting floods and evaluating water resources in karst areas ([Bonacci et al., 2006](#); Ford and Williams, 2007; Williams, [2008, 2009](#)). However, modelling floods in karst regions is extremely difficult because of the complex hydrogeological ~~structure~~structures of these regions. Karst water-bearing systems consist of multiple media ~~under the influence of~~and are influenced by complex karst development dynamics (Worthington et al., 2000; Kovács and Perrochet, 2008; [Gutierrez, 2010](#)), such as karst caves, conduits, fissures and pores, ~~and; thus, such systems~~ are usually highly spatially heterogeneous (Chang and Liu, 2015; [Mario Teixeira parente et al., 2019](#)). In addition, the ~~intricate~~complex surface hydrogeological conditions and the hydrodynamic conditions inside ~~the~~ karst water-bearing ~~medium~~media result in significant temporal and spatial differences in the hydrological processes in karst areas (Geyer et al., 2008; Bittner et al., 2020).

In early studies of flood forecasting in karst regions, simplified lumped hydrological models were commonly used to describe the rainfall–discharge relationship (e.g., Kovács and Sauter, 2007; Fleury et al., 2007b; Jukić and Denić, 2009; Hartmann et al., 2014a). With the development of physical exploration technology and the progress made in mathematics, computing and other interdisciplinary disciplines, the level of modelling has gradually

improved (Hartmann and Baker, 2017; Hartmann, 2018; Petrie et al., 2021), ~~and~~. Subsequently, distributed hydrological models have ~~subsequently become been~~ widely used in karst areas. The main difference between lumped and distributed hydrological models is that the latter divide the entire basin into many ~~sub-basins~~subbasins to ~~calculate the~~simulate runoff generation and confluence characteristics, thereby ~~better~~effectively describing the physical properties of the hydrological processes ~~inside the~~that occur in karst water-bearing system ~~(systems~~ (Jourde et al., 2007; Hartmann, 2018; Epting et al., 2018).

Because of their simple structure and ~~little~~low demand for modelling data, lumped hydrological models have been used widely in karst areas (Kurtulus and Razack, 2007; Ladouche et al., 2014). In a lumped model, ~~the~~a river basin is considered as a whole ~~to~~ ~~calculate the~~when simulating runoff generation and ~~confluence~~flow paths, and there is no division ~~running~~into ~~sub-basins~~subbasins (Dewandel et al., 2003; Bittner et al., 2020). Lumped models usually consider the inputs and outputs of the ~~model~~study area (Liedl and Sauter, 2003; Hartmann and Bake, 2013, 2017). In addition, most of the model parameters are not optimized in a lumped model, and the physical meaning of each parameter ~~is~~may be unclear (Chen, 2009; Bittner et al., 2020).

Distributed hydrological models are of ~~active~~high interest in flood simulation and forecasting research (Ambroise et al., 1996; Beven and Binley, 2006; Zhu and Li, 2014). Compared with ~~a~~-lumped ~~model, a~~models, distributed ~~model has a more definite~~models provide clear physical ~~significance for~~meaning regarding the model structure ~~in terms of its~~ ~~mechanism and~~ mechanisms (Meng and Wang, 2010; Epting et al., 2018). In a distributed hydrological model, an entire karst basin can be divided into many ~~sub-basins~~subbasins (Birk et al., 2005) using high-resolution digital elevation map (DEM) data. In the rainfall-runoff algorithm of ~~the~~a model, the hydrogeological conditions and karst aquifer characteristics can be fully considered ~~fully~~to ~~simulate~~precisely ~~the~~simulate runoff generation and ~~confluence~~(flow processes (Martinotti et al., 2017; Gang et al., 2019). ~~The commonly used~~Additionally, some basin-scale distributed hydrological models (~~i.e.~~not a ~~special~~specific groundwater numerical ~~model~~models, such as MODFLOW) have ~~also~~been applied ~~widely~~in karst areas, and ~~they~~ include the SHE/MIKE SHE model (Abbott et al.,

1986a,b; Doummar et al., 2012), the SWMM model (Peterson and Wicks, 2006; Blansett and Hamlett, 2010; Blansett, 2011), TOPMODEL (Ambroise et al., 1996; Suo et al., 2007; Lu et al., 2013; Pan, 2014) and the SWAT model (Peterson and Hamlett, 1998; Ren, 2006).

The commonly used distributed hydrological models have multiplevarious structures and numerous parameters (Lu et al., 2013; Pan, 2014), ~~which means that~~ a distributed model may ~~need~~require vast amounts of data to build ~~its~~ a framework for simulations in karst regions. For example, the distributed groundwater model MODFLOW-CFPM1 requires detailed data regarding the distribution of karst conduits in a study area (Reimann et al., 2009). Another example is the Karst–Liuxihe model (Li et al., 2019), ~~which has~~; notably, there are fifteen parameters and five underground vertical ~~layers~~structures in the model. Such a complex structure ~~and has 15 parameters, thereby making it difficult to model~~increases the data demand, and modelling in karst areas is extremely difficult. In addition, a special borehole pumping test may be required to obtain the rock permeability coefficient.

To overcome the ~~difficulty of the~~ large ~~modelling~~ data demands ~~for of~~ distributed hydrological models in karst areas, a new physically based distributed hydrological model—known as the QMG (Qingmuguan) model-V1.0—was developed in the present study. Other commonly used karst groundwater models with complex ~~structures~~structures and parameters—, such as the aforementioned MODFLOW-CFPM1 model—, require ~~a lot of~~considerable hydrogeological data for modelling in karst areas (Qin and Jiang, 2014). The new QMG model has ~~a~~ high potential for application in karst hydrological simulation and forecasting. ~~It, it~~ has certain advantages ~~in~~related to its framework and structural design, ~~having~~such as a double-layer structure and ~~fewer~~few parameters. The horizontal structure is divided into river channel units and slope units, and the vertical structure below the surface is divided into ~~a~~ shallow karst aquifer and ~~a~~ deep karst aquifer ~~systems~~systems. This relatively simple model structure reduces the demand for modelling data in karst areas, and ~~only a small amount of~~limited hydrogeological data ~~is~~are needed for modelling.—

~~To ensure that the QMG model work well in karst flood simulation and prediction in the~~

~~ease of relatively simple structure and parameters. We carefully designed the algorithms of runoff generation and confluence in the model.~~ To ensure that the QMG model works well in karst flood simulation and prediction despite its relatively simple structure and few parameters, we carefully designed the algorithms for runoff generation and ~~confluence~~flow in the model. ~~Also~~Additionally, to verify the applicability of the QMG model ~~to~~in flood simulation in karst basins, we selected the Qingmuguan karst trough valley in Chongqing, China, ~~as~~ the study area for ~~a~~ flood simulation and uncertainty analysis. In particular, we analysed the sensitivity of the model parameters.

2 Study area and data

2.1 Landform and topography

The Qingmuguan karst trough valley is located in the southeastern part of the Sichuan Basin, China, ~~at~~ the junction of the Beibei and Shapingba districts in Chongqing, with the coordinates ~~of~~ $29^{\circ}40'N-29^{\circ}47'N$; and $106^{\circ}17'E-106^{\circ}20'E$. The basin covers an area of 13.4 km^2 and is part of the southern extension of the anticline at Wintang Gorge in the Jinyun Mountains, with the anticlinal axis of Qingmuguan located in a parallel valley in eastern Sichuan (Yang et al., 2008). The surface of the anticline is heavily fragmented, and faults are extremely well developed with large areas of exposed Triassic carbonate rocks ~~exposed~~. Under the long-term erosion of karst water, a typical karst trough landform ~~pattern of 'three mountains and two troughs'~~ has formed, which looks like a pen-holder structure, means 'three ridges with two troughs' (Liu et al., 2009). This karst trough landform provides ~~convenient~~ideal conditions for flood propagation, and the development of karst landforms is extremely common in ~~the~~this karst region of ~~southwest~~Southwest China, especially in the karst region of ~~Chongqing. Similar regions include the karst trough valley of the Zhongliang Mountains and the Laolongdong karst basin in Nanshan,~~ Chongqing.

The basin is oriented ~~north-north-east and south-south-west~~ in a narrow band of slightly curved arcs and is $\sim 12\text{ km}$ long from north to south. The direction of the mountains in the region is ~~basically~~generally consistent with the ~~same as that~~direction of the tectonic line. ~~The~~

159 ~~difference in relative elevation is 200–300 m.~~ The map in ~~Fig.~~Figure 1 gives an overview of
160 the Qingmuguan karst basin.

161 **Figure 1.** The Qingmuguan karst basin.

162 2.2 Hydrogeological conditions

163 The Qingmuguan basin is located within the subtropical humid monsoon climate zone, with
164 an average temperature of 16.5°C and an average precipitation of 1250 mm ~~that is~~
165 concentrated mainly ~~in~~from May–September. An underground river system has developed in
166 the karst trough valley, with a length of 7.4 km, and the water supply of the underground
167 river is mainly rainfall recharge (Zhang, 2012). Most of the precipitation ~~is collected along~~
168 ~~the hill slope~~collects in hillslope areas and flows into the karst depressions at the bottom of
169 the trough valley, where it ~~is recharged~~provides recharge to the underground river through
170 ~~the dispersed infiltration~~ ~~of~~via surface karst fissures and ~~concentrated injection from~~
171 sinkholes (Fig. 1a). An upstream surface river ~~collects~~forms in a gentle valley and enters the
172 underground river through the Yankou sinkhole (elevation 524 m). Surface water in the
173 middle and lower reaches of the river system enters the underground river system mainly
174 through ~~even~~uniform cover-collapse sinkholes ~~or~~(Gutierrez et al., 2014) and fissures.

175 The stratigraphic and ~~lithologic~~lithological characteristics of the basin are dominated
176 largely by carbonate rocks of the Lower Triassic Jialingjiang Group (T_{1j}) and Middle
177 Triassic Leikou Slope Group (T_{2l}) on both sides of the slope, with some quartz sandstone
178 and mudstone outcrops of the Upper Triassic Xujiahe Group (T_{3xj}) (Zhang, 2012). The
179 topography of the basin presents a general anticline (Fig. 1b), where carbonate rocks on the
180 surface are corroded and fragmented, ~~with a large and have high~~ permeability ~~coefficient~~.
181 Compared with the core of the anticline, the ~~rocks of the two wings~~shale of the anticline
182 ~~are~~is less eroded and ~~form~~forms a good waterproof layer.

183 To investigate the distribution of karst conduits in the underground river system, we
184 conducted a tracer test in the study area. The tracer was placed into the Yankou sinkhole and
185 recovered in the Jiangjia spring (Fig. 1a,c). According to the tracer test results (Gou et al.,

2010), the karst water-bearing medium in the aquifer was anisotropic, ~~whereas the soluble~~
~~carbonate rocks were extremely permeable. The~~ karst conduits in the underground river
were extremely well developed, and there was a large single-channel underground river
~~approximately five metres wide.~~ The response of the underground river to rainfall was very
fast, with the peak flow observed at the outlet of Jiangjia spring 6–8 h after rainfall- ~~based on~~
~~the tracer test results.~~ The flood peak rose quickly, and the duration of the peak flow was
short. The underground river system in the study area is dominated by large karst conduits,
which ~~is~~are not conducive to water storage in water-bearing media, but ~~is~~are very conducive
to the propagation of floods.

2.3 Data

To build the QMG model to simulate ~~the~~ karst flood events, the necessary modelling
baseline data had to be collected, ~~including and they included~~ 1) high-resolution DEM data
and hydrogeological data (e.g., the thickness of the epikarst zone, rainfall infiltration
coefficient ~~on~~for different karst landforms, and permeability coefficient of rock); 2) land-
use and soil type data; and 3) rainfall data in the basin and water flow data ~~off~~for the
underground river. The DEM data ~~was~~were downloaded from a free internet database ~~on the~~
~~public Internet, with and had~~ an initial spatial resolution of 30×30 m. The spatial resolution
of ~~land use~~the land use and soil ~~types were type data was~~ 1000×1000 m, and ~~they~~these data
were also downloaded from the ~~Internet~~internet. After considering the applicability ~~of~~
~~modelling~~ and computational strength of the model, as well as the size of the basin in the
study area (13.4 km^2), the spatial resolution of the three types of data was resampled
uniformly in the QMG model and downscaled to 15×15 m based on ~~a~~the spatial discrete
method proposed by Berry et al. (2010).

The hydrogeological data necessary for modelling ~~was~~were obtained in three simple
ways. 1) A basin survey was conducted to obtain the thickness of the epikarst zone, which
was achieved by observing the rock formations on hillsides following cutting for road
construction. Information was collected regarding the location, general shape, and size of
karst depressions and sinkholes, ~~which had a significant impact on compiling the DEM data~~

and determining the convergence process of surface runoff, and these data were combined with DEM data and used to determine the convergence process of surface runoff. The sinkholes in the basin are cover-collapse sinkholes (Gutierrez et al., 2014) according to the basin survey. There are 3 large sinkholes (more than 3 metres in diameter) and 12 small sinkholes (less than 1 metre in diameter). The rest of the sinkholes, 5 in total, are between 1 and 3 metres in diameter. The confluence calculations for sinkholes in the model were based on the results of a previous study (Meng et al., 2009). 2) Empirical equations developed for similar basins were used to obtain the rainfall infiltration coefficient for different karst landforms and the permeability coefficient of rock. For example, the rock permeability coefficient was calculated based on an empirical equation ~~from~~ established based on a pumping test in a coal mine in the study area (Li et al., 2019, 2022). 3) A tracer experiment was conducted in the study area (Gou et al., 2010) to obtain information on the underground river direction and flow velocity; for instance, underground karst conduits are well developed in the area, and an underground river approximately five metres wide is present. There is no hydraulic connection between the underground river system in the area and the adjacent basin, which means that there is no overflow recharge.

Rainfall and flood data are important model inputs, and represent the driving factors that allow of hydrological models to operate. In the study area, rainfall data ~~was~~ were acquired ~~by~~ with two rain gauges located in the basin (Fig. 1a). Point rainfall was then spatially interpolated ~~into~~ to obtain basin-level rainfall (for such a small basin area, the rainfall results obtained from two rain gauges ~~was~~ were considered representative). There were 18 karst flood events ~~in the period of~~ from 14 April 2017 to 10 June 2019. We built a rectangular open channel at the underground river outlet and set up a river gauge ~~on it~~ in the channel (Fig. 1a) to record the water level and flow data every 15 minutes.

3 Methodology

3.1 Hydrological model framework and algorithms

The hydrological model developed in this study was named the QMG model after the basin for which it was developed and to which it was first applied, i.e., the Qingmuguan basin.

The QMG model ~~proposed in this study~~ has a two-layer structure, including a surface part and an underground part, ~~with the former. The surface part mainly performing~~ performs the ~~calculation of~~ runoff generation and surface routing calculations, and the underground part performs the ~~confluence of the surface river, while the latter performs the confluence~~ calculation of routing calculations for the underground river system.

The structure of the QMG model is divided into a two-layer structure, ~~both horizontally~~ with horizontal and ~~vertically~~ vertical components. The horizontal structure of the model is divided into river channel units and slope units. The vertical structure below the surface is divided into a shallow karst aquifer (including soil layers, karst fissures and conduit systems in the epikarst zone) and a deep karst aquifer system (~~rock stratum~~ bedrock and underground river system). ~~This~~ With this relatively simple model structure ~~means that,~~ only a small amount of hydrogeological data is needed ~~when modelling~~ in karst regions. Figure 2 shows a flowchart of the modelling and calculation procedures required for the QMG model.

Figure 2. Modelling flow chart of the QMG (Qingmuguan) model.

To ~~describe~~ accurately show the runoff generation and ~~confluence on a routing~~ processes at the grid scale, ~~these~~ the karst ~~sub-basins~~ subbasins are further divided into many karst hydrological response units (KHRUs) ~~based on the high-resolution (15 × 15 m) DEM data in the model.~~ The specific steps involved in the division were adopted by referring to ~~studies~~ a study of hydrological response units (HRUs) in TOPMODEL by Pan (2014). As the smallest basin units for computing ~~units, the,~~ KHRUs can effectively ~~ignore~~ mitigate the spatial differences ~~of~~ in karst development within ~~the~~ units and reduce the uncertainty in the classification of model units. Figure 3 shows the spatial structure of the KHRUs.

Figure 3. Spatial structure of karst hydrological response units (KHRUs) (Li et al., 2021).

The right-hand side of ~~Fig.~~ Figure 3 shows a three-dimensional spatial model of KHRUs established in the laboratory to ~~reflect~~ visually reflect the storage and movement of water in ~~the~~ karst water-bearing medium with ~~each~~ spatial anisotropy, and to provide technical support for establishing the hydrological model.

The modelling and operation of the QMG model ~~consists of~~ involve three main stages: 1)

spatial interpolation, and the ~~retention establishment~~ of rainfall and evaporation calculations;
 2) runoff generation and ~~confluence calculation~~ routing calculations for the surface river; and
 3) ~~confluence calculation~~ routing calculations for the underground runoff, including the
 confluence in the shallow karst aquifer and the underground river system.

3.1.1 Rainfall and evaporation ~~calculation~~ calculations

In the QMG model, the spatial interpolation of rainfall is accomplished ~~by~~ with a kriging method using the ArcGIS 10.2 software. ~~The Tyson~~ In some cases, the Thiessen polygon method may be a simpler method for rainfall interpolation if the number of rainfall gauges in the basin is sufficient. The point rainfall observed ~~by~~ with the two rainfall gauges in the basin (Fig. 1a) was interpolated spatially into areal rainfall for the entire basin.

Basin evapotranspiration in the KHRUs was mainly ~~vegetal, from vegetation, the soil evaporation~~ and water ~~surface evaporation. The~~ surfaces. These evapotranspiration components were calculated using the following equations (modified from Li et al., 2020):—

$$\begin{cases} E_v = V^{t+\Delta t} - V^t - P_v \\ E_s = \lambda E_p, \text{ if } F = F_c \\ E_s = \lambda E_p \frac{F}{F_c}, \text{ if } F < F_{\text{sat}} \\ E_w = \Delta e \cdot \left[1.12 + 0.62 (\Delta T)^{0.9} \right] \cdot \left[0.084 + 0.24 (1 - \gamma^2)^{1/2} \right] \cdot \left[0.348 + 0.5 \omega^{1.8-1.137 \omega^{0.05}} \right] \end{cases} \quad (1)$$

~~Here, where~~ E_v [mm] is the vegetal discharge, $V^{t+\Delta t} - V^t$ [mm] is the rainfall variation ~~by~~ due to vegetation interception, P_v [mm] is the ~~vegetation~~ interception of rainfall ~~by~~ ~~vegetation~~ and E_s [mm] is the actual soil evaporation. The term λ is the evaporation coefficient. The term E_p [mm] is ~~the potential~~ evaporation ~~capability~~, which can be measured experimentally or estimated ~~by the~~ with a water surface evaporation equation ~~for~~ E_w . The term F [mm] is the actual soil moisture, F_{sat} [mm] is the saturation moisture content, F_c [mm] is the field capacity, E_w [mm/d] is the evaporation ~~of the~~ from a water surface and ~~At~~ $\Delta e = e_0 - e_{150}$ [hPa] is the draught head between the saturation vapour pressure of ~~the~~ water surface and the air vapour pressure 150 m above the water

surface ~~(150 m above the water surface was selected here because the altitude for~~
~~temperature and humidity observations in the southwestern karst regions of China is~~
~~usually set at 150–200 m).~~ The term $\Delta T = t_0 - T_{150}$ [°C] is the temperature
difference between ~~the~~ water surface and ~~the temperature location~~ 150 m above the
water surface, γ is the relative humidity 150 m above the water surface and ω
[m/s] is the wind speed 150 m above the water surface.

3.1.2 Runoff generation

In the QMG model, the surface runoff generation in river channel units ~~means~~ is associated
with the rainfall in the basin that enters the river system after ~~deducting~~ subtracting
evaporation losses. This portion of the runoff ~~will participate~~ is directly involved in the
~~confluence~~ routing process ~~directly~~ through the river system, rather than undergoing
infiltration. In contrast, the process of runoff generation in slope units is more complex, and
~~its classification is~~ related to the developmental characteristics of the surface karst features
in the basin, the rainfall intensity and soil moisture. For example, when the soil ~~moisture~~
~~content is already~~ is saturated, there is the potential for excess infiltration -based surface
runoff in exposed karst slope units. ~~The surface~~ Surface runoff generation ~~of the KHRUs~~
~~the~~ river channel units and slope units in KHRUs can be described by the following
equations (modified from Chen, 2009, 2018; Li et al., 2020):

$$\left\{ \begin{array}{l} P_r(t) = [P_i(t) - E_p] \frac{L \cdot W_{\max}}{A} \\ R_{si} = (P_i - f_i), P_i > f_{\max} \\ R_{si} = 0, P_i < f_{\max} \\ f_{\max} = \alpha(F_c - F)^\beta + F_s \end{array} \right\} \left\{ \begin{array}{l} P_r(t) = [P_i(t) - E_p] \frac{L \cdot W_{\max}}{A} \\ R_{si} = (P_i - f_i), P_i \geq f_{\max} \\ R_{si} = 0, P_i < f_{\max} \\ f_{\max} = \alpha(F_c - F)^\beta + F_s \end{array} \right. \quad (2)$$

~~Here, where~~ $P_r(t)$ [mm] is the net rainfall (~~deducting~~ subtracting evaporation losses) in the
river channel units at time t [h], $P_i(t)$ [mm] is the rainfall in the river channel units, L [m] is
the length of the river channel, W_{\max} [m] is the maximum width of the river channel
selected and A [m²] is the cross-sectional area of the river channel. R_{si} [mm] is ~~termed~~ the
excess infiltration runoff in the QMG model, when the vadose zone is ~~short of water and has~~

~~not been filled. The nonsaturated. Notably, the~~ infiltration capacity f_{\max} ~~is different~~ varies in different karst landform units, α , ~~and~~ β are the parameters of the Holtan model, and F_s [mm] is the stable depth of soil water infiltration.

In the KHRUs (Fig. 3), underground runoff is generated primarily from the infiltration of rainwater and direct confluence recharge from sinkholes or ~~skylights~~ karst windows. In the QMG model, ~~the~~ underground runoff is calculated by the following equations (modified from Chen, 2018):

$$\begin{cases} R_g = R_0 \exp(-pt^m) \\ R_e = v_e \cdot I_w \cdot z \end{cases} \begin{cases} R_g = R_0 \exp(-pt^m) \\ R_e = v_e \cdot I_w \cdot z \end{cases} \quad (3)$$

where—

$$\begin{cases} \frac{\partial R_e}{\partial x} + I_w \cdot z \cdot \frac{\partial F}{\partial t} = R_r - R_{\text{epi}} \\ v_e = K \cdot \tan(\alpha), \quad F > F_c \\ v_e = 0, \quad F \leq F_c \end{cases} \quad (4)$$

Here, R_g [mm] is the underground runoff depth (this part of ~~the~~ underground runoff is mainly directly from ~~the direct confluence supply of the~~ karst sinkholes or ~~skylights~~ karst windows in the study area), R_0 [mm] is the average depth of ~~the~~ underground runoff, p and m are attenuation coefficients that were calculated by conducting a tracer test in the study area, R_e [L/s] is the underground runoff generated from rainfall infiltration in the epikarst zone, I_w [mm] is the width of the underground runoff ~~on~~ zone in the KHRUs, z [mm] is the thickness of the epikarst zone, R_r [mm²/s] is the runoff-based recharge ~~on~~ in the KHRUs during period t , R_{epi} [mm²/s] is the water infiltration from rainfall, v_e [mm/s] is the flow velocity of ~~the~~ underground runoff, K [mm/s] is the ~~current~~ permeability coefficient and ~~α~~ α is the hydraulic gradient of ~~the~~ underground runoff. If the ~~current~~ soil moisture level is less than the field capacity, ~~i.e. $F \leq F_c$, then $F \leq F_c$~~ , and the vadose zone is not yet full, there will be no underground runoff generation, and rainfall infiltration ~~at this time~~ will continue to compensate for the lack of water in fill the vadose zone ~~until it is full and~~ before it becomes

saturated, at which point runoff is generated.

3.1.3 Channel routing and ~~confluence~~convergence

In the QMG model, ~~the calculation of~~ runoff ~~confluence on the~~routing in KHRUs includes the confluence of ~~the~~ surface river channel and underground runoff. There are already many ~~mature and classical~~classic algorithms available for ~~calculating the~~performing runoff ~~confluence~~routing calculations in river channel units and slope units, such as the Saint-Venant equations and Muskingum convergence model. In this study, the Saint-Venant equations were adopted to ~~describe the confluence in~~assess flow routing for the surface river and ~~in~~ hill slope units, ~~for which and~~ a wave movement equation was adopted ~~to~~ ~~calculate confluence~~for convergence calculations in slope units (Chen, 2009):

$$\left\{ \begin{array}{l} \frac{\partial Q}{\partial x} + L \frac{\partial h}{\partial t} = q \\ S_f - S_0 = 0 \end{array} \right. \left\{ \begin{array}{l} \frac{\partial Q}{\partial x} + L \frac{\partial h}{\partial t} = q \\ S_f - S_0 = 0 \end{array} \right. \quad (5)$$

where—

$$Q = v h L = \frac{L}{n} h^{\frac{5}{3}} S_0^{\frac{1}{2}}. \quad (6)$$

Here, we customized two variables a and b :

$$\left\{ \begin{array}{l} a = \left(\frac{n}{L} S_0^{-\frac{1}{2}} \right)^{\frac{3}{5}} \\ b = \frac{3}{5} \end{array} \right. \left\{ \begin{array}{l} a = \left(\frac{n}{L} S_0^{-\frac{1}{2}} \right)^{\frac{3}{5}} \\ b = \frac{3}{5} \end{array} \right. \quad (7)$$

Equation (7) was substituted into Eq.-(5) and discretized ~~by~~with a finite-difference method, ~~giving~~yielding

$$\left\{ \begin{array}{l} \frac{\partial Q}{\partial x} + a b Q^{(b-1)} \frac{\partial Q}{\partial t} - q = 0 \\ \frac{\Delta t}{\Delta x} Q_{i+1}^{t+1} + a (Q_{i+1}^{t+1})^b = \frac{\Delta t}{\Delta x} Q_i^{t+1} + a (Q_{i+1}^t)^b + q_{i+1}^{t+1} \Delta t \end{array} \right.$$

$$\begin{cases} \frac{\partial Q}{\partial x} + abQ^{(b-1)} \frac{\partial Q}{\partial t} - q = 0 \\ \frac{\Delta t}{\Delta x} Q_{i+1}^{t+1} + a(Q_{i+1}^{t+1})^b = \frac{\Delta t}{\Delta x} Q_i^{t+1} + a(Q_i^t)^b + q_{i+1}^{t+1} \Delta t \end{cases} \quad (8)$$

The Newton–Raphson method was used for the iterative calculation using Eq.-(8):

$$\begin{aligned} [Q_{i+1}^{t+1}]^{k+1} &= [Q_{i+1}^{t+1}]^k - \frac{\frac{\Delta t}{\Delta x} [Q_{i+1}^{t+1}]^k + a([Q_{i+1}^{t+1}]^k)^b - \frac{\Delta t}{\Delta x} Q_i^{t+1} - a(Q_i^t)^b - q_{i+1}^{t+1} \Delta t}{\frac{\Delta t}{\Delta x} + ab([Q_{i+1}^{t+1}]^k)^{b-1}} \\ [Q_{i+1}^{t+1}]^{k+1} &= [Q_{i+1}^{t+1}]^k - \frac{\frac{\Delta t}{\Delta x} [Q_{i+1}^{t+1}]^k + a([Q_{i+1}^{t+1}]^k)^b - \frac{\Delta t}{\Delta x} Q_i^{t+1} - a(Q_i^t)^b - q_{i+1}^{t+1} \Delta t}{\frac{\Delta t}{\Delta x} + ab([Q_{i+1}^{t+1}]^k)^{b-1}} \end{aligned} \quad (9)$$

where Q [L/s] is the ~~confluence~~ convergence of water flow in slope units, L [dm] is ~~its the~~ width of the runoff ~~width~~ zone in a slope unit, h [dm] is the runoff depth and q [dm²/s] is the lateral inflow ~~on~~ in the KHRUs. Here, the friction slope ~~S_f~~ S_f equals the hill slope ~~S_0~~ S_0 , and the inertia term and the pressure term in the motion equation of the Saint-Venant ~~equation~~ equation set were ignored. The term v [dm/s] is the flow velocity of surface runoff in the slope units, as calculated by the Manning equation. Additionally, n is the roughness coefficient of the slope units, ~~Q_i^{t+1}~~ Q_i^{t+1} [L/s] is the slope inflow in ~~the~~ a KHRU at time $t+1$ and ~~Q_{i+1}^{t+1}~~ Q_{i+1}^{t+1} [L/s] is the slope discharge in the upper adjacent KHRU at time $t+1$.

Similarly, ~~the~~ surface river channel ~~confluence~~ convergence was described based on the Saint-Venant ~~equation, where equations, and~~ a diffusion wave movement equation was adopted, ~~meaning that; therefore,~~ the inertia term in the motion equation was ignored:-

$$\begin{cases} \frac{\partial Q}{\partial x} + \frac{\partial A}{\partial t} = q \\ S_f = S_0 - \frac{\partial h}{\partial x} \end{cases} \begin{cases} \frac{\partial Q}{\partial x} + \frac{\partial A}{\partial t} = q \\ S_f = S_0 - \frac{\partial h}{\partial x} \end{cases} \quad (10)$$

A finite-difference method and the Newton–Raphson method were used ~~for the iterative~~ to iteratively solve the above equation:-

$$\begin{cases}
\left[Q_{i+1}^{t+1} \right]^{k+1} = \left[Q_{i+1}^{t+1} \right]^k - \frac{\frac{\Delta t}{\Delta x} \left[Q_{i+1}^{t+1} \right]^k + c \left(\left[Q_{i+1}^{t+1} \right]^k \right)^b - \frac{\Delta t}{\Delta x} Q_i^{t+1} - c (Q_{i+1}^t)^b - q_{i+1}^{t+1} \Delta t}{\frac{\Delta t}{\Delta x} + cb \left(\left[Q_{i+1}^{t+1} \right]^k \right)^{b-1}} \\
c = \left(\frac{1}{3600} n \chi^{\frac{2}{3}} S_f^{-\frac{1}{2}} \right)^{\frac{3}{5}}
\end{cases} \quad \text{set:}$$

$$\begin{cases}
\left[Q_{i+1}^{t+1} \right]^{k+1} = \left[Q_{i+1}^{t+1} \right]^k - \frac{\frac{\Delta t}{\Delta x} \left[Q_{i+1}^{t+1} \right]^k + c \left(\left[Q_{i+1}^{t+1} \right]^k \right)^b - \frac{\Delta t}{\Delta x} Q_i^{t+1} - c (Q_{i+1}^t)^b - q_{i+1}^{t+1} \Delta t}{\frac{\Delta t}{\Delta x} + cb \left(\left[Q_{i+1}^{t+1} \right]^k \right)^{b-1}} \\
c = \left(\frac{1}{3600} n \chi^{\frac{2}{3}} S_f^{-\frac{1}{2}} \right)^{\frac{3}{5}}
\end{cases} \quad (11)$$

where Q [L/s] is the water flow in surface river channel units, A [dm²] is the cross-sectional area of discharge, c is a custom intermediate variable and χ [dm] is the wetted perimeter of the discharge cross-section area.

The underground runoff area in the model includes the confluence convergence region of the epikarst zone and underground river. In the epikarst zone, the karst water-bearing media are highly heterogeneous. (Williams, 2008). For example, the crisscrossed anisotropic karst fissure systems and conduit systems consist of large corrosion fractures. When rainfall infiltrates into the epikarst zone, water moves slowly through the small (less than 10 cm in this study) karst fissure systems, while and it flows rapidly in larger (more than 10 cm) conduits. The key to determining the confluence flow velocity lies in determining the width of karst fractures. In the KHRUs (Fig. 3), the 10-cm fracture width of the fracture 10 cm was used as a threshold value (Atkinson, 1977), meaning that based on a borehole pumping test in the basin. Thus, if the fracture width exceeded 10 cm, then the water movement into it in the fracture was defined as rapid flow; otherwise, it was defined as slow flow. The confluence flow in the epikarst zone was calculated by the following equation (modified from Beven and Binley, 2006):

$$Q(t)_{ijk} = b_{ijk} \cdot \frac{\Delta h}{\Delta l} R_i C_j \cdot T(t)_{\text{slow/rapid}} \quad Q(t)_{ijk} = b_{ijk} \cdot \frac{\Delta h}{\Delta l} R_i C_j \cdot T(t)_{\text{slow/rapid}}$$

where

398

$$\begin{cases} T(t)_{\text{slow}} = nr \frac{\rho g R_i C_j L_k}{12\nu} \\ T(t)_{\text{rapid}} = \frac{K_{ij} (e^{-f_{ij} h_{ij}} - e^{-f_{ij} z_{ij}})}{f_{ij}} \end{cases} \quad (13)$$

399

Here, $\underline{Q(t)_{ijk}}$ [L/s] is the flow ~~confluence~~ in the epikarst zone at time t , $\underline{b_{ijk}}$

400

[dm] is the width of the runoff ~~width~~ zone, $\frac{\Delta h}{\Delta l}$ is the dimensionless hydraulic gradient,

401

$T(t)_{\text{slow/rapid}}$ is the dimensionless hydraulic conductivity, $\underline{\rho}$ [g/L] is the density of ~~the~~

402

water ~~flow~~, g [m/s²] is gravitational acceleration, n is the number of valid computational

403

units, $\underline{R_i C_j L_k}$ [L] is the volume of the ijk -th KHRU, ν is the kinematic viscosity

404

coefficient, f_{ij} is the attenuation coefficient in the epikarst zone, h_{ij} [dm] is the depth of

405

shallow groundwater and z_{ij} [dm] is the thickness of the epikarst zone.

406

The distinction between rapid and slow flows in the epikarst zone is not absolute. ~~The~~

407

~~10-cm-width-of-a-karst~~ Notably, the established fracture ~~as the dividing~~ threshold ~~also has~~

408

~~some subjectivity of 10 cm may be unrepresentative because pumping tests were conducted~~

409

in only five boreholes in the region. In fact, there is usually water exchange between the

410

rapid and slow ~~flows~~ flow zones at the ~~junction~~ junctions of large and small fissures in karst

411

aquifers. In the QMG model, this water exchange can be described with ~~this~~ the following

412

equation (modified ~~form~~ from Li et al., 2021):

413

$$\begin{cases} Q = \alpha_{i,j,k} (h_n - h_{i,j,k}) \\ \alpha_{i,j,k} = \sum_{ip=1}^{np} \frac{(K_w)_{i,j,k} \pi d_{ip} \frac{1}{2} (\Delta l_{ip} \tau_{ip})}{r_{ip}} \end{cases} \begin{cases} Q = \alpha_{i,j,k} (h_n - h_{i,j,k}) \\ \alpha_{i,j,k} = \sum_{ip=1}^{np} \frac{(K_w)_{i,j,k} \pi d_{ip} \frac{1}{2} (\Delta l_{ip} \tau_{ip})}{r_{ip}} \end{cases}$$

414

(14)

415

Here, $\alpha_{i,j,k}$ [dm²/s] is the water exchange coefficient in the ijk -th KHRU, $\underline{(h_n - h_{i,j,k})}$

416

$\underline{(h_n - h_{i,j,k})}$ [dm] is the water head difference between the rapid and slow ~~flows~~ flow zones

417

at the junction of large and small fissures in KHRUs, np is the number of fissure systems

418

connected to the adjacent conduit systems, $\underline{(K_w)_{i,j,k}}$ [dm/s] is the permeability

coefficient at the junction of a fissure and conduit, $\frac{d_{ip}}{d_{ip}}$ and $\frac{r_{ip}}{r_{ip}}$ [dm] are the conduit diameter and radius, respectively; $\frac{\Delta l_{ip}}{\Delta l_{ip}}$ [dm] is the length of the connection between conduits i and p , and $\frac{\tau_{ip}}{\tau_{ip}}$ is the conduit curvature. Some of the parameters in this equation, such as $\frac{(K_w)_{i,j,k}}{(K_w)_{i,j,k}}$ and $\frac{(h_n - h_{i,j,k})}{(h_n - h_{i,j,k})}$, were obtained by conducting an infiltration test in the study area.

The ~~confluence of convergence patterns in~~ the underground river system ~~playshave~~ an important ~~role for influence on~~ the ~~confluence flow regime~~ at the basin outlet. To facilitate the ~~calculation of confluence routing calculations~~ in the QMG model, the underground river ~~systemssystem~~ can be generalized into large multiple-conduit systems. During floods, these conduit systems are mostly under pressure. Whether the water flow is laminar or turbulent depends on the flow regime at that time. The water flow into these conduits is calculated ~~bybased on~~ the Hagen–Poiseuille equation and the Darcy–Weisbach equation (Shoemaker et al., 2008):

$$\begin{cases} Q_{\text{laminar}} = -A \frac{gd^2 \partial h}{32\nu \partial x} = -A \frac{\rho g d^2 \Delta h}{32\mu \tau \Delta l} \\ Q_{\text{turbulent}} = -2A \sqrt{\frac{2gd|\Delta h|}{\Delta l \tau}} \log \left(\frac{H_c}{3.71d} + \frac{2.51\nu}{d \sqrt{\frac{2gd^3|\Delta h|}{\Delta l \tau}}} \right) \frac{\Delta h}{|\Delta h|} \end{cases}$$

$$\begin{cases} Q_{\text{laminar}} = -A \frac{gd^2 \partial h}{32\nu \partial x} = -A \frac{\rho g d^2 \Delta h}{32\mu \tau \Delta l} \\ Q_{\text{turbulent}} = -2A \sqrt{\frac{2gd|\Delta h|}{\Delta l \tau}} \log \left(\frac{H_c}{3.71d} + \frac{2.51\nu}{d \sqrt{\frac{2gd^3|\Delta h|}{\Delta l \tau}}} \right) \frac{\Delta h}{|\Delta h|} \end{cases} \quad (15)$$

Here, $\frac{Q_{\text{laminar}}}{Q_{\text{laminar}}}$ [L/s] is ~~the water flow of~~ the laminar flow in the conduit systems, A [dm²] is the conduit cross-sectional area, d [dm] is the conduit diameter, $\frac{\rho}{\rho}$ [kg/dm³] is the density of ~~the underground riverwater~~, $\frac{\nu = \mu / \rho}{\nu = \mu / \rho}$ is the coefficient of

kinematic viscosity, $\frac{\Delta h}{\tau \Delta l}$ is the hydraulic slope of the conduits, τ is the dimensionless conduit curvature, $\frac{Q_{\text{turbulent}}}{Q_{\text{turbulent}}}$ [L/s] is the turbulent flow in the conduit systems and H_c [dm] is the average conduit wall height.

3.2 Parameter optimization

In total, the QMG model has 12 parameters, of which flow direction and slope are topographic parameters that can be determined from the DEM without parametric optimization, while the remaining 10 parameters require calibration. Other distributed hydrological models with multiple structures usually have many parameters. For example, the Karst–Liuxihe model (Li et al., 2021) has 15 parameters that must be calibrated. In the QMG model, each parameter is normalized as

$$x_i = x_i^* / x_{i0}, \quad (16)$$

where x_i is the dimensionless parameter value for i after it is normalized, x_i^* is the parameter value for i in actual physical units, and x_{i0} is the initial or final value of x_i . Through the processing of Eq. (16), the value range of the model parameters is limited to a hypercube $K_n = (X \mid 0 \leq x_i \leq 1, i = 1, 2, \dots, n)$, and K is a dimensionless value. This normalized treatment ignores the influence of the spatiotemporal variation of the underlying surface attributes on the parameters, while also simplifying the parameter classification and the number of the model parameters to a certain extent. Accordingly, the model parameters can be further divided into rainfall-evaporation parameters, epikarst-zone parameters and underground-river parameters. Table 1 lists the parameters of the QMG model.

Table 1. Parameters of the QMG model.

Because the QMG model has relatively few parameters, it is possible to calibrate them manually, which has the advantage that the operation is easy to implement and does not require a special program for parameter optimization. However, the disadvantage is that this manual approach is subjective, which can lead to great uncertainty in the manual parameter calibration process. To compare the effects of parameter optimization on model

performance, ~~this study used~~ both manual parameter calibration and the improved chaotic particle swarm optimization algorithm (IPSO) were used for the automatic calibration of model parameters, and ~~compared~~ the effects of both on flood simulation were compared.

In general, the structure and parameters of a standard particle swarm optimization algorithm (PSO) are simple, with the initial parameter values obtained at random. For parameter optimization in high-dimensional ~~multi-peak~~multipeak hydrological models, the standard PSO is easily limited to ~~a~~-local convergence and cannot achieve the optimal effect, ~~while~~and the late evolution of the algorithm may also cause problems, such as ~~preconity~~ and premature convergence or stagnant evolution, due to the ‘inert’ aggregation of particles, which seriously affects the efficiency of parameter selection. It is necessary to overcome the above problems ~~and makeso that~~ the algorithm can converge to the global optimal solution with a high probability. In parameter optimization for the QMG model, we improved the standard PSO algorithm by adding chaos theory, and developed the IPSO, ~~where method;~~ notably, 10 cycles of chaotic disturbances were added to improve the activity of the particles. The inverse mapping equation ~~offor~~ the chaotic variable is

$$\begin{cases} X_{ij} = X_{\min} + (X_{\max} - X_{\min}) * Z_{ij} \\ Z'_{ij} = (1 - \alpha)Z^* + \alpha Z_{ij} \end{cases} \quad (17)$$

where X_{ij} is the optimization variable for the model parameters, ~~($X_{\max} - X_{\min}$)~~ ($X_{\max} - X_{\min}$) is the difference between ~~its~~the maximum and ~~its~~-minimum values of X_{ij} , Z_{ij} is the variable before the disturbance is added ~~and~~, Z'_{ij} ~~representsis~~ is the chaotic ~~variables~~variable after a disturbance is added, ~~α~~ α is a variable determined by the adaptive algorithm, ($0 \leq \alpha \leq 1$), and Z^* is the chaotic variable formed when the optimal particle ~~mapsis mapped~~ to the interval [0,1]. ~~In parameter optimization, the~~The flowchart of ~~the~~ IPSO is shown in Fig.Figure 4.

Figure 4. Algorithm flow chart of IPSO.

3.3 Uncertainty analysis

Uncertainties in hydrological model simulation results usually originate from three ~~aspects:factors:~~ the input data, the model structure and the model parameters (Krzysztofowicz, 2014). In the present study, the input data (e.g., rainfall, flood ~~events~~ and ~~some~~ hydrogeological data) were first validated and ~~pre-processed through~~ preprocessed based on observations to reduce ~~their uncertainties~~ uncertainty.

Second, we simplified the structure of the QMG model to reduce the structural uncertainty. As a mathematical and physical model, a hydrological model ~~has~~ is characterized by some uncertainty in flood simulation and forecasting because of the errors in the system structure and ~~the~~ selected algorithm (Krzysztofowicz and Kelly, 2000). The model in this study was designed with full consideration of the relationship between the amount of data required to build the model and ~~its~~ model performance ~~for~~ in flood simulation and forecasting in karst regions, ~~and the model's.~~ The entire model framework was integrated through simple structures and easy-to-implement algorithms, ~~using~~ based on the concept of distributed hydrological modelling. Conventionally, the ~~extent~~ level of uncertainty ~~is~~ increased increases with the growing complexity of the model structure. We therefore ensured that the structure of the QMG model was simple when it was designed, and the double-layer model was divided into surface and underground ~~double-layer~~ structures to reduce ~~its~~ structural uncertainty.

Third, we ~~focus~~ focused on analysing the uncertainty and sensitivity of ~~the~~ model parameters and ~~their~~ the applied optimization method, ~~for which;~~ specifically, a ~~multi-parametri~~ multiparametric sensitivity analysis method (Choi et al., 1999; Li et al., 2020) was used to analyse the sensitivity of the parameters in the QMG model. The steps in the parameter sensitivity analysis are as follows.

1) Selection of the appropriate objective function

The Nash–Sutcliffe coefficient is widely used ~~as the objective function~~ to evaluate the performance of hydrological models (Li et al., 2020, 2021). ~~It was~~; therefore, it was used to assess the QMG model in this study. Because the most important factor in flood forecasting

is the peak discharge, it is used in the Nash coefficient equation:

$$NSC = 1 - \frac{\sum_{i=1}^n (Q_i - Q'_i)^2}{\sum_{i=1}^n (Q_i - \bar{Q})^2}, \quad (18)$$

where NSC is the Nash–Sutcliffe coefficient, Q_i [L/s] ~~are~~is the observed flow ~~discharges~~discharge, Q'_i [L/s] ~~are~~is the simulated ~~discharges~~discharge, \bar{Q} [L/s] is the average observed discharge and n [h] is the observation period.

2) Parameter sequence sampling

The Monte Carlo sampling method was used to sample 8000 groups of parameter sequences. The parametric sensitivity of the QMG model was analysed and evaluated by comparing the differences between the a priori and a posteriori distributions of the parameters.

3) Parameter sensitivity assessment

The a priori distribution of a model parameter ~~means~~is its probability distribution, ~~while~~and the a posteriori distribution refers to the conditional distribution calculated after sampling, which can be calculated based on the ~~simulation result~~results of the ~~parametric parameter~~ optimization. If there is a significant difference between ~~them~~the a priori distribution and the a posteriori distribution of a parameter, then the parameter being tested ~~has~~is characterized by high sensitivity; ~~whereas; conversely,~~ if there is no obvious difference, then the parameter is insensitive. The ~~parametric~~a priori distribution of a parameter is calculated as

$$\begin{cases} P_{i,j}(NSC_{i,j} \geq 0.85) = \frac{n}{N+1} \times 100 \\ \sigma_i = \sum_{j=1}^n (P_{i,j} - \bar{P}_{i,j})^2 \end{cases} \quad (19)$$

where $P_{i,j}$ is the ~~a priori distribution's~~ probability associated with a given a priori distribution when ~~$NSC_{i,j} \geq 0.85$~~ $NSC_{i,j} \geq 0.85$. We used a simulated Nash coefficient of 0.85 as the threshold value, and n was the number of occurrences of a Nash coefficient greater than 0.85

in flood simulations. In each simulation, only a certain parameter was changed, ~~while~~ and the remaining parameters remained unchanged. If the Nash coefficient of ~~this~~ simulation exceeded 0.85, then the flood simulation results were considered acceptable. The term σ_i is the difference between ~~the~~ acceptable value and ~~its~~ the overall mean, which represents the parametric sensitivity ($0 < \sigma_i < 1$). The higher the σ_i value is, the more sensitive the parameter. ~~N is~~ In this study, N denotes the 8000 parameter sequences, and $\overline{P_{i,j}}$ is the average value of the a priori distribution.

3.4 ~~Model Settings~~ Settings

~~Once~~ After the model was built and before it was run, some of the initial conditions ~~had to be set before running it to simulate and forecast floods~~, such as the basin division scheme, the ~~setting of~~ initial soil moisture levels, and the ~~assumption of the~~ initial parameter ~~rangeranges, were set~~. 1) In the study area, the entire Qingmuguan karst basin was divided into 893 KHRUs, including 65 surface river units, 466 hill slope units, and 362 underground river units. The division of these units formed the basis for ~~calculating the process of~~ runoff generation and convergence- calculations. 2) The initial soil moisture level was set to 0–100% of the ~~saturation~~ saturated moisture content in the basin, and the specific soil moisture level before each flood ~~had to be~~ was determined ~~by~~ through a trial calculation. 3) The ~~waterhead~~ hydraulic head boundary conditions ~~off~~ for the groundwater zone were determined by a tracer test in the basin, ~~where~~ and a perennial stable water level in area adjacent to the groundwater- divide was used as the fixed ~~waterhead~~ head value at the model boundary. The base flow of the underground river was determined to be 35 L/s ~~from~~ based on the perennial average dry season runoff. 4) The ~~rangeranges~~ of initial parameters and the convergence conditions were ~~assumed~~ set before parameter optimization (Figure 4). 5) Parameter optimization and flood simulation ~~validated~~ were performed to validate the performance of the QMG model in karst basins.

4 Results and discussion

4.1 Parameter Sensitivity Resultssensitivity results

The number of parameters in a distributed hydrological model is generally large, and it is important to perform a sensitivity analysis of each parameter to quantitatively assess the impact of the different parameters on model performance. In the QMG model, each parameter was divided into four categories according to its sensitivity: (i) highly sensitive, (ii) sensitive, (iii) moderately sensitive, and (v) insensitive. In the calibration of model parameters, insensitive ~~ones~~parameters do not need to be calibrated, which can greatly reduce the ~~amount~~number of ~~calculation~~calculations and improve the efficiency of model ~~operation~~operations.

The flow process in the calibration period (14 April to 10 May 2017) was adopted to calculate the sensitivity of the model parameters, ~~for which the calculation principle was and~~ ~~calculations were based on~~ equation (19), ~~and the~~. The parameter sensitivity results are ~~calculated~~listed in Table 2.

Table 2 Parametric sensitivity results ~~in~~for the QMG model.

In Table 2, the value of ~~σ_i~~ σ_i [equation (19)] represents a parameter's sensitivity, and the higher the value is, the more sensitive the parameter ~~is~~. ~~From the~~. The results in Table 2; ~~it was found~~ indicate that the rainfall infiltration coefficient, rock permeability coefficient, rock porosity, ~~and the related~~ parameters ~~of~~related to the soil water content, such as the saturated water content, and field capacity, ~~were~~are sensitive parameters. The order of parameter sensitivity ~~was~~is as follows: infiltration coefficient > permeability coefficient > rock porosity > specific yield > saturated water content > field capacity > flow direction > thickness > slope > ~~Soil~~soil coefficient > channel roughness > evaporation coefficient.

In the QMG model, parameters are classified as highly sensitive, sensitive, moderately sensitive, and insensitive according to their influence on the flood simulation results. In Table 4, we ~~divided~~divide the sensitivity of model parameters into four levels based on the ~~σ_i~~ σ_i value: 1) highly sensitive parameters, $0.8 < \sigma_i < 1$; 2) sensitive parameters,

0.65 < σ_i < 0.8; 3) moderately sensitive parameters, 0.45 < σ_i < 0.65; and 4) insensitive parameters, 0 < σ_i < 0.45. The highly sensitive parameters were the infiltration coefficient, permeability coefficient, rock porosity, and specific yield. The sensitive parameters were the saturated water content, field capacity, and thickness of the epikarst zone. The moderately sensitive parameters were the flow direction, slope, and soil coefficient. The insensitive parameters were channel roughness and the evaporation coefficient.

4.2 Parametric Optimization

In total, the QMG model has 12 parameters, of which only eight need to be optimized, which is relatively few for distributed models. The parameters of flow direction and slope as well as the insensitive parameters of, as channel roughness and the evaporation coefficient, which are insensitive parameters, need not be calibrated; this approach can improve the convergence efficiency of the model parameter optimization process.

In the study area, 18 karst floods during the period of from 14 April 2017 to 10 June 2019 were recorded at the underground river outlet to validate the effects of the QMG model in karst hydrological simulations. The calibration period was 14 April to 10 May 2017 at the beginning of the flow process, with the remainder of the time being period used as the validation period. In the QMG model, the IPSO algorithm was used to optimize the model parameters. To show demonstrate the necessity of need for parameter optimization for the distributed hydrological model, the study specifically compared the flood simulation results obtained using the initial parameters of the model (without parameter calibration) and the optimized parameters. Figure 5 shows the iterative parameter optimization process for the QMG model.

Figure 5 Iterative parameter optimization process.

Figure 5 shows that almost all parameters fluctuated widely considerably fluctuate at the beginning of the optimization, and then after about approximately 15 iterations of the iterative optimization calculations, most of the linear fluctuations become significantly less volatile variable, which indicates that the algorithm tends to

converge (possibly only locally). When the number of iterations exceeded 25, all parameters remained essentially unchanged, ~~meaningsuggesting~~ that the algorithm ~~had~~ converged (at this point ~~there was~~, global convergence was achieved). It took only 25 iterations to ~~reach~~ ~~achieve~~ definite convergence ~~of-for parameters in~~ the ~~parameter rates with this applied~~ IPSO algorithm, ~~which; thus, this approach~~ is extremely efficient in terms of ~~the~~ parameter optimization ~~offor~~ distributed hydrological models. In previous studies of the ~~parametric~~ optimization ~~forof the parameters of~~ the Karst-Liuxihe model in similar basin areas, 50 ~~automatic-parameter-optimization-iterations~~ iterative steps were required to reach convergence in automatic parameter optimization (Li et al., 2021), demonstrating the effectiveness of the IPSO algorithm.

To evaluate the effect of parameter optimization, the convergence efficiency of the algorithm, and, more importantly, the parameters after calibration were ~~used to simulate~~ ~~floods. Fig-~~ assessed in flood simulation cases. Figure 6 shows the flood simulation ~~effects~~ results.

Figure 6 Flow simulation results of the QMG model based on parameter optimization.

~~Fig-~~ Figure 6 shows that the flows simulated ~~byfollowing~~ parameter optimization were better than those ~~simulated byobtained with~~ the initial model parameters. The simulated flow ~~processes~~ values based on the initial parameters were relatively small, with the simulated peak flows ~~in-particular-being~~ notably smaller than the observed values, ~~and; additionally,~~ there were large errors between the ~~twosimulated and observed~~ values. In contrast, the simulated flows produced by the QMG model after parameter optimization were very similar to the observed values, which indicates that calibration of the model parameters ~~iswas~~ necessary and that there was an improvement in parameter optimization achieved through the use of the IPSO algorithm in this study. In addition, ~~it was found that~~ the flow simulation effect was better in the calibration periods than in the validation periods (Fig. 6).

To compare the results of the flow ~~processes-simulation~~ process simulations with the initial model parameters and the optimized parameters, six evaluation indices (Nash–Sutcliffe coefficient, correlation coefficient, relative flow process error, flood peak error,

water balance coefficient, and peak time error) were applied in this study, and the results are presented in Table 3.

Table 3 Flood simulation evaluation ~~index through~~indices following parametric optimization.

Table 3 shows that the evaluation indices of the flood simulations after ~~parametric~~parameter optimization were better than those ~~of~~obtained with the initial model parameters. The average values of the initial parameters for these six indices were 0.81, 0.74, 27%, 31%, 0.80, and 5 h, respectively. For the optimized parameters, the average values were 0.90, 0.91, 16%, 14%, 0.94, and 3 h, respectively. The flood simulation effects after parameter optimization clearly improved, implying that parameter optimization for the QMG model is necessary, and that the IPSO algorithm for parameter optimization is an effective approach that can greatly improve the convergence efficiency of parameter optimization, and ~~also~~ ensure that the model performs well in flood simulations.

4.3 Model ~~Validation~~validation in Flood Simulationsflood simulations

Following parameter optimization, we simulated the whole flow process (14 April 2017 to 10 June 2019-) based on the optimized and initial parameters of the QMG model (Fig. ~~6~~, ~~which enabled a visual reflection of the model used in the simulation of~~6). This approach allowed us to visually assess a long series of flow processes obtained with the model. To reflect the simulation effect of the model for different flood events, we divided the whole flow process into 18 flood events, and then used the initial parameters of the model and the optimized parameters, ~~respectively~~, to verify the model performance in flood simulations. ~~Fig.~~Figure 7 and Table 4 show the flood simulation effects and ~~their~~the calculated evaluation indices using both the initial and ~~the~~ optimized parameters.

Figure 7 Flood simulation effects based on the initial and optimized parameters.

Table 4 Flood simulation indices for model validation.

~~Fig.~~Figure 7 shows that the flood simulation ~~results~~values obtained using the initial parameters were smaller than the observed values, and the model performance improved in flood simulations after parameter optimization. The simulated flood processes were in good

agreement with observations, and flood peak flows were especially ~~effective for simulating~~
~~flood peak flows, well simulated.~~ From the flood simulation indices in Table 4, the average
water balance coefficient based on the initial parameters was 0.69, i.e., much less than 1,
indicating that the simulated water in the model was unbalanced. After parameter
optimization, the average value was 0.92, indicating that parameter optimization had a
significant impact on the ~~model~~-water balance calculation.

Table 4 shows that the average values of the six indices (Nash–Sutcliffe coefficient,
correlation coefficient, relative flow process error, flood peak error, water balance
coefficient, and peak time error) for the initial parameters were 0.79, 0.74, 26%, 25%, 0.69,
and 5 h, respectively, while for the optimized parameters, the average values were 0.92, 0.90,
10%, 11%, 0.92, and 2 h, respectively. All evaluation indices improved after parameter
optimization, with the average values of the Nash coefficient, correlation coefficient, and
water balance coefficient increasing by 0.13, 0.16, and 0.23, respectively. ~~The~~Additionally,
the average values of the relative flow process error, flood peak error, and peak time error
decreased by 15%, 14%, and 3 h, respectively. These reasonable flood simulation results
confirmed that parameter optimization ~~by~~with the IPSO algorithm was necessary and
effective for the QMG model.

Compared with the overall flow process simulation shown in Figure 6, each flood
process was better simulated by the QMG model (Fig. 7). ~~This was because~~Notably, in the
~~function of the~~-QMG model and ~~its~~the applied algorithm-~~design~~, the main consideration ~~was~~
~~the calculation of the~~-is flood process, ~~but~~ calculations, and the correlation algorithm ~~of~~
~~the~~for dry-~~season~~ runoff was not sufficiently described ~~well enough~~. For example,
equations (12)–(15) are used in the flood convergence algorithm. ~~As a result~~Consequently,
the model is not good at simulating other flow processes, such as dry-~~season~~ runoff, leading
to ~~a~~-low accuracy in simulations of the overall flow process. The next phase of our research
will focus on refining the algorithm related to dry-~~season~~ runoff and improving the
comprehensive performance of the model.

4.4 Uncertainty analysis

4.4.1 Assessment and reduction of uncertainty

In general, the uncertainty in model simulation is due mainly to three ~~aspects of the~~ ~~model factors~~: (i) the uncertainty of ~~its~~ input data, (ii) the uncertainty of ~~its~~ the model structure and algorithm and (iii) the uncertainty of ~~its~~ the model parameters. In the practical application of a hydrological model, these three uncertainties are usually interwoven, which leads to ~~the~~ overall uncertainty ~~of~~ in the final simulation results (Krzysztofowicz, 2014). Therefore, ~~the present~~ this study focused on the uncertainties in the input data, the model structure and the parameters to reduce the overall uncertainty of the simulation results.

First, the input data—mainly rainfall-runoff data and hydrogeological data—were ~~pre-processed,~~ preprocessed, which substantially reduced their uncertainty. Second, we simplified the structure of the QMG model, ~~which is reflected in the fact that it has~~ with only two structural layers ~~of spatial structure~~ in the horizontal and vertical directions. This relatively simple structure greatly reduced ~~greatly~~ the modelling uncertainty ~~due to the model structure.~~ In contrast, ~~the underground structure of~~ our previous Karst–Liuxihe model (Li et al., 2021) ~~has~~ included five layers, which ~~leads~~ led to ~~great~~ considerably uncertainty. Third, appropriate algorithms for runoff generation and confluence were selected. ~~Different~~ In general, different models ~~were~~ are designed for different purposes, which leads to ~~great~~ notable differences in the algorithms used. In the QMG model, most of the rainfall-runoff algorithms used have been validated by the research results of others, and some of them were improved ~~to suit~~ for karst flood simulation and forecasting ~~by~~ with the QMG model. For example, the algorithm for the generation of excess infiltration runoff [Eq.-(2)] was an improvement of the version used in the Liuxihe model (Chen, 2009, 2018; Li et al., 2020). Finally, the algorithm for parameter optimization was improved. Considering the shortcomings of the standard PSO algorithm ~~that,~~ which tends to converge locally, ~~this study developed the~~ IPSO for parameter optimization was developed in this study by adding chaotic perturbation factors. The flood simulation results after parameter optimization were much better than those ~~of~~ obtained with the initial model parameters (Figs. 6 and 7 and Tables 2 and 3), which indicates that parameter optimization is necessary

for ~~a~~-distributed hydrological ~~model~~models and can reduce the uncertainty of ~~the~~ model parameters.

4.4.2 ~~Parameter sensitivity~~ Sensitivity analysis

The parameter-sensitivity results in Table 2 show that the rainfall-infiltration coefficient in the QMG model was the most sensitive parameter. ~~It and~~ was the key to ~~determining~~ the generation of excess infiltration surface runoff and ~~separating~~the separation of surface runoff from subsurface runoff. If the rainfall infiltration coefficient ~~was~~is greater than the infiltration capacity, excess infiltration surface runoff ~~was~~will be generated on ~~the~~-exposed karst landforms; otherwise, all rainfall ~~would~~will infiltrate ~~to meet the water deficit in~~into the vadose zone, and then continue to seep-~~down~~ into the underground river system, eventually flowing out of the basin through the underground river outlet. The ~~confluence~~flow modes of surface runoff and underground runoff were completely different, resulting in a large difference in the simulated flow results. Therefore, the rainfall infiltration coefficient had the greatest impact on the final flood simulation results.

Other highly sensitive parameters, such as the rock permeability coefficient, rock porosity and specific yield, were used as the basis for dividing between slow flow in karst fissures and rapid flow in conduits. The division of slow and rapid flows also had a ~~great~~considerable impact on the discharge at the outlet of the basin. Slow flow plays an important role in water storage in ~~a~~-karst ~~aquifer~~aquifers and is very important for the replenishment of river base flow in the dry season. Rapid flow in large conduit systems dominates ~~the~~-flood runoff and is the main component of the flood water volume in the flood season.

Parameters related to the soil water content, including the saturated water content, field capacity and thickness, were sensitive parameters and had a large influence on the flood simulation results. ~~This is because~~Notably, the soil moisture content prior to flooding affects how flood flows rise and when peaks occur. If the soil is already very wet or even saturated before ~~the~~-flooding, ~~the~~a flood will rise quickly ~~to~~and reach a peak, and the ~~process line of~~ ~~the~~-flood peak flow will be sharp and ~~thin~~short. This type of flood ~~process forms~~can easily

759 ~~occur~~ and can lead to ~~a~~ disaster-causing flood ~~event~~event. In contrast, if the soil in the basin
760 is very dry before ~~the~~ flooding, the rainfall will first ~~meet the water shortage of~~saturate the
761 vadose zone, ~~and after it is replenished; then~~, the rainfall will infiltrate into the underground
762 river. The flood peak ~~of~~at the river basin outlet is therefore delayed.

763 The moderately sensitive parameters were ~~the~~ flow direction, slope and ~~the~~ soil
764 coefficient. ~~They; they~~ had a specific influence on the flood simulation results, but the
765 influence was not as great as that of the highly sensitive and sensitive parameters. The
766 insensitive parameters were channel roughness and the evaporation coefficient. The amount
767 of water lost ~~by~~via evapotranspiration is very small ~~in~~compared to the total volume of flood
768 water, and ~~it~~evapotranspiration was therefore the least ~~—~~sensitive parameter in the QMG
769 model.

770 5 Conclusions

771 ~~This~~In this study ~~proposed~~, a new distributed physically based hydrological model, i.e., the
772 QMG model, was proposed to accurately simulate floods ~~accurately~~ in karst trough and
773 valley landforms. The main conclusions of this paper are as follows.

774 ~~This~~The QMG model has ~~a~~ high application potential in karst hydrology simulations.
775 Other distributed hydrological models usually have multiple structures, resulting in the need
776 for a large amount of data to build models in karst areas (Kraller et al., 2014). The QMG
777 model has only a double-layer structure, with ~~a~~ clear physical meaning, and a small amount
778 of basic data ~~is needed to build the model in karst areas~~, such as some necessary
779 hydrogeological data, is needed to build the model in karst areas. For example, the
780 distribution and flow direction of underground rivers ~~is required, which must be known and~~
781 can be inferred from ~~a~~ tracer ~~test, leading to a~~tests at low ~~modelling~~ cost. There ~~were~~are
782 fewer parameters in the QMG model than in other distributed hydrological models, with
783 only 10 parameters that ~~needed~~need to be calibrated.

784 The flood ~~simulations~~simulations after parameter optimization ~~was~~were much better
785 than ~~the simulation using those based on~~ the initial model parameters. After parameter
786 optimization, the average values of the Nash coefficient, correlation coefficient and water

balance coefficient increased by 0.13, 0.16 and 0.23, respectively, ~~while~~ and the average relative flow process error, flood peak error and peak time error decreased by 15%, 14% and 3 h, respectively. Parameter optimization is necessary for ~~a~~-distributed hydrological ~~model~~models, and the ~~improvement of the~~improved IPSO algorithm in this study was ~~an~~ effective ~~way to achieve this~~.

In the QMG model, the rainfall infiltration coefficient I_c , the rock permeability coefficient K , the rock porosity R_p and the parameters related to the soil water content were sensitive parameters. The order of parameter sensitivity was infiltration coefficient > permeability coefficient > rock porosity > specific yield > saturated water content > field capacity > flow direction > thickness > slope > soil coefficient > channel roughness > evaporation coefficient.

This QMG model is suitable for karst trough and valley ~~basins~~landforms, such as those in the study area, where the topography is conducive to the spread of flood water. ~~Whether~~In the future, it must be verified whether this model is applicable to other karst areas ~~in non-trough valley regions still needs to be verified in the future studies and landforms~~. In addition, although the studied basin area is very small, ~~where~~but the hydrological similarity ~~between~~among different small basin areas varies greatly (Kong and Rui, 2003). The size of the area to be modelled has a great influence on the choice of ~~model~~-spatial resolution for modelling (Chen et al., 2017). Therefore, it must be determined whether the QMG model is suitable for flood forecasting in large karst basins ~~needs to be determined~~.

Model development.

~~This~~The QMG model presented in this study uses ~~the~~ Visual Basic language programming. The general framework of the model and the algorithm consist of three parts: the ~~modeling~~modelling approach, the ~~algorithm of~~ rainfall-runoff generation and ~~confluence~~convergence algorithm, and the parameter optimization algorithm. As a free and open-source hydrological ~~modeling~~modelling program (QMG model-V1.0), we provide all ~~modeling~~modelling packages, including the model code, installation package, simulation data package and user manual, free of charge. It is important to note that the model we provide ~~are~~is for scientific research purposes only and should not be used for any commercial purposes. ~~— (Creative Commons Attribution 4.0 International-).~~
~~Model~~The model installation program can be downloaded from ZENODO, ~~cite~~Zenodo and should be cited as (JI LI. (2021, June 16). QMG model-V1.0. Zenodo.

<http://doi.org/10.5281/zenodo.4964701>, and <http://doi.org/10.5281/zenodo.4964697> (registration required). ~~User~~The user manual can be downloaded from <http://doi.org/10.5281/zenodo.4964754>.–

Code availability.

All ~~code~~codes for the QMG model-V1.0 in this paper are available and free, and the code can be downloaded from ~~ZENODO, Cite as JI LI. (2021, June 16). QMG model-V1.0 code (Version v1.0). Zenodo.~~ at <http://doi.org/10.5281/zenodo.4964709> (registration required) ~~(Cite as JI LI. (2021, June 16). QMG model-V1.0 code (Version v1.0). Zenodo).~~

Data availability.–

All data used in this paper are available, findable, accessible, interoperable, and reusable. The simulation data and modelling data package can be downloaded from <http://doi.org/10.5281/zenodo.4964727>. The DEM was downloaded from the Shuttle Radar Topography Mission database at <http://srtm.csi.cgiar.org>. The land use-type data were downloaded from <http://landcover.usgs.gov>, –and the soil-type data were downloaded from <http://www.isric.org>. These data were last accessed on 15 October 2020.

Author contributions. JIL was responsible for the calculations and writing of the whole paper. DY helped conceive the structure of the model. ZF and JL provided significant assistance in the English translation of the paper. MM provided flow data ~~off~~from the study area.–

Competing interests.

The authors declare that they have no conflicts of interest.

~~Acknowledgments~~Acknowledgements.

This study was supported by the National Natural Science Foundation of China (41830648), the National Science Foundation for Young Scientists of China (42101031), the Fundamental Research Funds for the Central Universities (), Chongqing Natural Science Foundation (cstc2021jcyj-msxm0007), and the Chongqing Education Commission Science and ~~technology~~Technology ~~research~~Research Foundation (KJQN202100201), the ~~drought monitoring, analysing~~Drought Monitoring, Analysis and ~~early~~Early ~~warning of typical prone to drought areas of~~Warning Project

849 for Typical Drought-Prone Areas in Chongqing (20C00183~~7~~) and the Open Project Program
850 of the Guangxi Key Science and Technology Innovation Base on Karst Dynamics (KDL &
851 Guangxi 202009, KDL & Guangxi 202012).

References

- Abbott, M. B., Bathurst, J. C., Cunge, J. A., O'Connell, P. E., and Rasmussen, J.: An Introduction to the European Hydrologic System-System Hydrologue European, 'SHE', a: History and Philosophy of a Physically-based, Distributed Modelling System, J. Hydrol., 87, 45–59, 1986a.
- Abbott, M. B., Bathurst, J. C., Cunge, J. A., O'Connell, P. E., and Rasmussen, J.: An Introduction to the European Hydrologic System-System Hydrologue European, 'SHE', b: Structure of a Physically based, distributed modeling System, J. Hydrol., 87, 61–77, 1986b.
- Ambroise, B., Beven, K., and Freer, J.: Toward a generalization of the TOPMODEL concepts: Topographic indices of hydrologic similarity. Water Resources Research, 32, 2135-2145, 1996.
- Atkinson, T.C.: Diffuse flow and conduit flow in limestone terrain in the Mendip Hills, Somerset (Great Britain). Journal of Hydrology, 35, 93-110. [https://doi.org/10.1016/0022-1694\(77\)90079-8](https://doi.org/10.1016/0022-1694(77)90079-8), 1977.
- Berry, R.A., Saurel, R., and Lemetayer, O.: The discrete equation method (DEM) for fully compressible, two-phase flows in ducts of spatially varying cross-section. Nuclear Engineering & Design, 240(11), 3797-3818, 2010.
- Beven, K., and Binley, A.: The future of distributed models: Model calibration and uncertainty prediction. Hydrological Processes, 6, 279-298, 2006.
- Birk, S., Geyer, T., Liedl, R., and Sauter, M.: Process-based interpretation of tracer tests in carbonate aquifers. Ground Water, 43(3), 381-388, 2005.
- Bittner, D., Parente, M.T., Mattis, S., Wohlmuth, B., and Chiogna, G.: Identifying relevant hydrological and catchment properties in active subspaces: An inference study of a lumped karst aquifer model. ADVANCES IN WATER RESOURCES, 135, 550-560. [doi: 10.1016/j.advwatres.2019.103472](https://doi.org/10.1016/j.advwatres.2019.103472), 2020.

878 Blansett, K. L., and Hamlett, J. M.: Challenges of Stormwater Modeling for Urbanized Karst
879 Basins. Pittsburgh, Pennsylvania, an ASABE Meeting Presentation, Paper Number:
880 1009274. [doi:10.13031/2013.29840](https://doi.org/10.13031/2013.29840), 2010.

881 Blansett, K. L.: Flow, water quality, and SWMM model analysis for five urban karst basins..
882 (Doctoral dissertation). The Pennsylvania State University, USA, 2011.

883 Bonacci, O., Ljubenkov, I., and Roje-Bonacci, T.: Karst flash floods: an example from
884 the Dinaric karst Croatia. Nat. Hazards Earth Syst. Sci. 6, 195–203, 2006.

885 Chang, Y., and Liu, L.: A review of hydrological models in karst areas. Engineering
886 investigation, 43,37-44, 2015.

887 Chen, G.M., Jia, J.Y., and Han, Q.: Research on inertia weight reduction strategy of Particle
888 Swarm optimization algorithm. Journal of Xi'an Jiaotong University, 40(1),53-56, 2006.

889 Choi, J., Harvey, J. W., and Conklin, M. H.: Use of multi-parameter sensitivity analysis to
890 determine relative importance of factors influencing natural attenuation of mining
891 contaminants. the Toxic Substances Hydrology Program Meeting, Charleston, South
892 Carolina, 1999.

893 Chen, Y. B.: Liuxihe Model, China Science and Technology Press, Beijing, China, 2009.

894 Chen, Y., Li, J., and Xu, H.: Improving flood forecasting capability of physically based
895 distributed hydrological models by parameter optimization. Hydrol. Earth Syst. Sci. 20,
896 375-392. <https://doi.org/10.5194/hess-20-375-2016>, 2016.

897 Chen, Y., Li, J., Wang, H., Qin, J., and Dong, L.: Large watershed flood forecasting with
898 high-resolution distributed hydrological model. Hydrol. Earth Syst. Sci. 21, 735-749.
899 <https://doi.org/10.5194/hess-21-735-2017>, 2017.

900 Chen, Y.: Distributed Hydrological Models. Springer Berlin Heidelberg, Berlin, Germany.
901 https://doi.org/10.1007/978-3-642-40457-3_23-1, 2018.

902 Dewandel, B., Lachassagne, P., Bakalowicz, M., Weng, P., and Malki, A.A.: Evaluation of
903 aquifer thickness by analysing recession hydrographs. Application to the Oman

ophiolite hard-rock aquifer. *Journal of Hydrology*, 274,248-269, 2003.

Dubois, E., Doummar, J., Séverin Pistre, S., and Larocque, M.: Calibration of a lumped karst system model and application to the Qachqouch karst spring (Lebanon) under climate change conditions. *Hydrol. Earth Syst. Sci.*, 24, 4275-4290. <https://doi.org/10.5194/hess-24-4275-2020>, 2020.

Doummar, J., Sauter, M., and Geyer, T.: Simulation of flow processes in a large scale karst system with an integrated catchment model (MIKE SHE) – identification of relevant parameters influencing spring discharge. *Journal of Hydrology*, 426-427, 112-123, 2012.

Epting, J., Page, R.M., and Auckenthaler, A.: Process-based monitoring and modeling of Karst springs–Linking intrinsic to specific vulnerability. *Science of the Total Environment*, 625, 403-415, 2018.

Fleury, P., Plagnes, V., and Bakalowicz, M.: Modelling of the functioning of karst aquifers with a reservoir model: Application to Fontaine de Vaucluse (South of France). *Journal of Hydrology*, 345,38-49. <http://dx.doi.org/10.1016/j.jhydrol.2007.07.014>, 2007b.

Ford, D. C., and Williams, P.W.: *Karst geomorphology and hydrology*. Wiley, Chichester, England, 2007.

Gang, L., Tong, F.G., and Bin,T.: A Finite Element Model for Simulating Surface Runoff and Unsaturated Seepage Flow in the Shallow Subsurface. *Hydrological Processes*, 6,102-120. doi: 10.1002/hyp.13564, 2019.

Geyer, T., Birk, S., Liedl, R., and Sauter, M.: Quantification of temporal distribution of recharge in karst systems from spring hydrographs. *Journal of Hydrology*, 348(30), 452-463, 2008.

Gou, P.F., Jiang, Y.J., Hu, Z.Y., Pu, J.B., and Yang, P.H.: A study of the variations in hydrology and hydrochemistry under the condition of a storm in a typical karst subterranean stream. *HYDROGEOLOGY&ENGINEERING GEOLOGY*,37(5),20-25, 2010.

- Gutierrez, F.: Hazards associated with karst. In: Alcantara, I. & A. Goudie (Eds.),
Geomorphological Hazards and Disaster Prevention. Cambridge University Press,
Cambridge, 161–175, 2010.
- Gutierrez, F., Parise, M., D' Waele, J., and Jourde, H.: A review on natural and human-
induced geohazards and impacts in karst. *Earth Science Reviews*, 138, 61-88, 2014.
- Hartmann, A., and Baker, A.: Progress in the hydrologic simulation of time variant of karst
systems-Exemplified at a karst spring in Southern Spain. *Advances in Water Resources*,
54,149-160, 2013.
- Hartmann, A., Goldscheider, N., Wagener, T., Lange, J., and Weiler, M.: Karst water
resources in a changing world: Review of hydrological modeling approaches. *Reviews
of Geophysics* 52: 218-242. doi: [10.1002/2013RG000443](https://doi.org/10.1002/2013RG000443), 2014a.
- Hartmann, A., and Baker, A.: Modelling karst vadose zone hydrology and its relevance for
paleoclimate reconstruction. *Earth-Science Reviews*, 172, 178-192, 2017.
- Hartmann, A.: Experiences in calibrating and evaluating lumped karst hydrological models.
London: Geological Society, Special Publications, 2018.
- Jourde, H., Roesch, A., Guinot, V., and Bailly-Comte, V.: Dynamics and contribution of
karst groundwater to surface flow during Mediterranean flood. *Environ. Geol.* 51 (5),
725–730, 2007.
- Jourde, H., Lafare, A., Mazzilli, N., Belaud, G., Neppel, L., Doerfliger, N., and Cernesson, F.:
Flash flood mitigation as a positive consequence of anthropogenic forcings on the
groundwater resource in a karst catchment. *Environ. Earth Sci.* 71, 573–583,2014.
- Jukić, D., and Denić-Jukić, V.: Groundwater balance estimation in karst by using a
conceptual rainfall–runoff model. *Journal of Hydrology*, 373, 302-315.
<http://dx.doi.org/10.1016/j.jhydrol.2009.04.035>, 2009.
- Kong, F.Z., and Rui, X.F.: Hydrological similarity of catchments based on topography.

956 GEOGRAPHICAL RESEARCH, (06), 709-715, 2003.

957 Kovács, A., and Sauter, M.: Modelling karst hydrodynamics. In: Goldscheider N, Drew D
 958 (eds) Methods in karst hydrogeology, IAH international contributions to hydrogeology;
 959 26,264 p, 2007.

960 Kovács, A., and Perrochet, P.: A quantitative approach to spring hydrograph decomposition.
 961 Journal of Hydrology, 352, 16-29. <http://dx.doi.org/10.1016/j.jhydrol.2007.12.009>,
 962 2008.

963 Kurtulus, B., and Razack, M.: Evaluation of the ability of an artificial neural network model
 964 to simulate the input-output responses of a large karstic aquifer: the la rochefoucauld
 965 aquifer (charente, france). Hydrogeology Journal, 15(2), 241-254, 2007.

966 Krzysztofowicz, R., and Kelly, K.: Hydrologic uncertainty processor for probabilistic river
 967 stage forecasting. Water Resources Research, 36(11),3265-3277, 2000.

968 Krzysztofowicz, R.: Probabilistic flood forecast : Exact and approximate predictive
 969 distributions. Journal of Hydrology, 517(1), 643-651, 2014.

970 Kraller, G., Warscher, M., Strasser, U., Kunstmann, H., and Franz, H.: Distributed
 971 hydrological modeling and model adaption in high alpine karst at regional scale
 972 (berchtesgaden alps, germany). Springer International Publishing Switzerland.
 973 https://doi.org/10.1007/978-3-319-06139-9_8, 2014.

974 Ladouche, B., Marechal, J. C., and Dorfliger, N.: Semi-distributed lumped model of a karst
 975 system under active management. Journal of Hydrology, 509,215-230, 2014.

976 Li, J., Chen, Y., Wang, H., Qin, J., Li, J., and Chiao, S.: Extending flood forecasting lead
 977 time in a large basin by coupling WRF QPF with a distributed hydrological model,
 978 Hydrol. Earth Syst. Sci. 21, 1279–1294. <https://doi.org/10.5194/hess-21-1279-2017>,
 979 2017.

980 Li, J., Yuan, D., Liu, J., Jiang, Y., Chen, Y., Hsu, K. L., and Sorooshian, S.: Predicting floods
 981 in a large karst river basin by coupling PERSIANN-CCS QPEs with a physically based
 982 distributed hydrological model. Hydrol. Earth Syst. Sci. 23, 1505-1532.

<https://doi.org/10.5194/hess-23-1505-2019>, 2019.

Li, J., Hong, A., Yuan, D., Jiang,Y., Deng,S., Cao,C., and Liu, J.: A new distributed karst-tunnel hydrological model and tunnel hydrological effect simulations. Journal of Hydrology, 593, 125639. <https://doi.org/10.1016/j.jhydrol.2020.125639>, 2020.

Li, J., Hong, A., Yuan, D., Jiang,Y., Zhang,Y., Deng,S., Cao,C., Liu, J., and Chen,Y.: Elaborate Simulations and Forecasting of the Effects of Urbanization on Karst Flood Events Using the Improved Karst-Liuxihe Model.CATENA,197,104990. <https://doi.org/10.1016/j.catena.2020.104990>, 2021.

Li, J., Yuan, D., Ma, M., and Liu, J.: Simulation of Karst Floods with a Hydrological Model Improved by Meteorological Model Coupling, Journal of Hydrometeorology, 23(2),185-207. doi: 10.1175/JHM-D-21-0088.1, 2022.

Liedl, R., Sauter, M., Huckinghaus, D., Clemens, T., and Teutsch, G.: Simulation of the development of karst aquifers using a coupled continuum pipe flow model. Water Resources Research, 39, 50-57, 2003.

Liu, X., Jiang, Y.J., Ye, M.Y., Yang, P.H., Hu, Z.Y., and Li, Y.Q.: Study on hydrologic regime of underground river in typical karst valley- A case study on the Qingmuguan subterranean stream in Chongqing. CARSOLOGICA SINICA, 28(2),149-154, 2009.

Lu, D. B., Shi, Z. T., Gu, S. X., and Zeng, J. J.: Application of Hydrological Model in the Karst Area. Water-saving irrigation.11, 31-34. [doi:1007-4929\(2013\)11-031-04](https://doi.org/10.1007/4929(2013)11-031-04), 2013.

~~Mario, T.P., Daniel, B., Steven, A. M., Gabriele, C., and Barbara, W~~

Martinotti, M.E., Pisano, L., Marchesini, I., Rossi, M., Peruccacci, S., Brunetti, M.T., Melillo, M.,Amoruso, G., Loiacono, P., Vennari, C., Vessia, G., Trabace, M., Parise, M., and Guzzetti, F.: Landslides, floods and sinkholes in a karst environment: the 1–6 September 2014 Gargano event, southern Italy. Natural Hazards and Earth System Sciences, 17, 467-480, 2017.

Meng, H.H., Wang, N.C., Su, W.C., and Huo, Y.: Modeling and application of karst semi-distributed hydrological model based on sinkholes. SCIENTIA GEOGRAPHICA

[SINICA, 5, 550-554. doi: 10.3969/j.issn.1000-0690.2009.04.014, 2009.](#)

~~Bayesian calibration and sensitivity analysis for a karst aquifer model using active subspaces. Water Resources Research, 55,342-356. doi: 10.1029/2019WR024739, 2019.~~

Meng, H.H., and Wang, N.C.: Advances in the study of hydrological models in karst basin. Progress in Geography, 29,1311-1318, 2010.

Pan, H.Y.: Hydrological model and application in karst watersheds. China University of Geosciences. Doctoral Dissertation, Wuhan, China, 2014.

[Parise, M.: Hazards in karst, Proceedings Int. Conf. “Sustainability of the karst environment. Dinaric karst and other karst regions”, IHP-Unesco, Series on Groundwater,2, 155-162, 2010.](#)

Peterson, E.W., and Wicks, C. M.: Assessing the importance of conduit geometry and physical parameters in karst systems using the storm water management model (SWMM).Journal of Hydrology, 329, 1-2, 294-305, 2006.

Peterson, J.R., and Hamlett, J.M.: Hydrologic calibration of the SWAT model in a basin containing fragipan soils. JAWRA Journal of the American Water Resources Association. doi: 10.1111/j.1752-1688.1998.tb00952.x, 1998.

Petrie, R., Denvil, S., Ames, S., et al.: Coordinating an operational data distribution network for CMIP6 data, Geosci. Model Dev., 14, 629–644, <https://doi.org/10.5194/gmd-14-629-2021>, 2021.

Qin, J.G., and Jiang, Y.P.: A review of numerical simulation methods for CFP pipeline flow. Groundwater. 3, 98-100, 2014.

Reimann, T., Melissa, E., and Hill.: Modflow-cfp: a new conduit flow process for modflow– 2005. Ground Water,47(3),321-325. doi:10.1111/j.1745-6584.2009.00561.x, 2009.

Ren, Q.W.: Water Quantity Evaluation Methodology Based on Modified SWAT Hydrological Modeling in Southwest Karst Area, China University of Geoscience,

1036 Wuhan, China, 2006.

1037 Shoemaker, W.B., Cunningham, K.J., and Kuniansky, E.L.: Effects of turbulence on
 1038 hydraulic heads and parameter sensitivities in preferential groundwater flow layers.
 1039 Water Resources Research, 44, 34-50. doi: [10.1029/2007WR006601](https://doi.org/10.1029/2007WR006601), 2008.

1040 Suo, L.T., Wan, J.W., and Lu, X.W.: Improvement and application of TOPMODEL in karst
 1041 region. Carsologica Sinica, 26(1), 67-70, 2007.

1042 Teixeiraparente, M., Bittner, D., Mattis, S.A., Chiogna, G., and Wohlmuth, B.:
 1043 Bayesian calibration and sensitivity analysis for a karst aquifer model using active
 1044 subspaces. Water Resources Research, 55, 342-356. doi: [10.1029/2019WR024739](https://doi.org/10.1029/2019WR024739),
 1045 2019.

1046 White, W.B.: Karst hydrology: recent developments and open questions. Eng. Geol. 65, 85–
 1047 105, 2002.

1048 Williams, P.W.: The role of the epikarst in karst and cave hydrogeology: a review. Int. J.
 1049 Speleol. 37, 1–10, 2008.

1050 Williams, P. W.: Book Review: Methods in Karst Hydrogeology, Nico Goldscheider and
 1051 David Drew (eds). Hydrogeology Journal, 17,1025-1025, 2009.

1052 Worthington, S., Ford, D., and Beddows, P.: Porosity and permeability enhancement in
 1053 unconfined carbonate aquifers as a result of solution. Speleogenesis: evolution of karst
 1054 aquifers, 2000.

1055 Yang, P. H., Luo, J.Y., Peng, W., Xia, K.S., and Lin, Y.S.: Application of online technique in
 1056 tracer test-A case in Qingmuguan subterranean river system, Chongqing, China.
 1057 CARSOLOGICA SINICA, 27(3),215-220, 2008.

1058 Yu, D., Yin, J., Wilby, R.L., Stuart, N. L., Jeroen, C., Lin, N., Liu, M., Yuan, H., Chen, J.,
 1059 Christel, P., Guan, M., Avinoam, B., Charlie, W. D., Tang, X., Yu, L., and Xu, S.:
 1060 Disruption of emergency response to vulnerable populations during floods. Nature
 1061 Sustainability, 3, 728–736. <https://doi.org/10.1038/s41893-020-0516-7>, 2020.

- 1062 Yu, Q., Yang, P.H., Yu, Z.L., Chen, X.B., and Wu, H.: Dominant factors controlling
1063 hydrochemical variation of karst underground river in different period,
1064 Qingmuguan, Chongqing. *CARSOLOGICA SINICA*, 35(2), 134-143, 2016.
- 1065 Zhang, Q.: Assessment on the intrinsic vulnerability of karst groundwater source in the
1066 Qingmuguan karst valley. *CARSOLOGICA SINICA*, 31(1), 67-73, 2012.
- 1067 Zhu, C., and Li, Y.: Long-Term Hydrological Impacts of Land Use/Land Cover Change
1068 From 1984 to 2010 in the Little River Basin, Tennessee. *International Soil and Water*
1069 *Conservation Research*, 2(2), 11-21, 2014.

Tables

Table 1 Parameters of the QMG model.

Parameters	Variable name	Physical property
Infiltration coefficient	I_c	Meteorology Meteorological
Evaporation coefficient	λ	Vegetation cover
Soil thickness	h	Karst aquifer
Soil coefficient	S_b	Soil type
Saturated water content	S_c	Soil type
Rock porosity	R_p	Karst aquifer
Field capacity	F_c	Soil type
Permeability coefficient	K	Karst aquifer
Flow direction	F_d	Landform
Slope	S_0	Landform
Specific yield	S_y	Karst aquifer
Channel roughness	n	Landform

Table 2 Parametric sensitivity results in the QMG model.

I_c	λ	h	S_b	S_c	S_y	F_d	S_0	R_p	F_c	K	n
0.92	0.24	0.71	0.58	0.8	0.83	0.74	0.68	0.86	0.78	0.89	0.36

Table 3 Flood simulation evaluation index through parametric optimization.

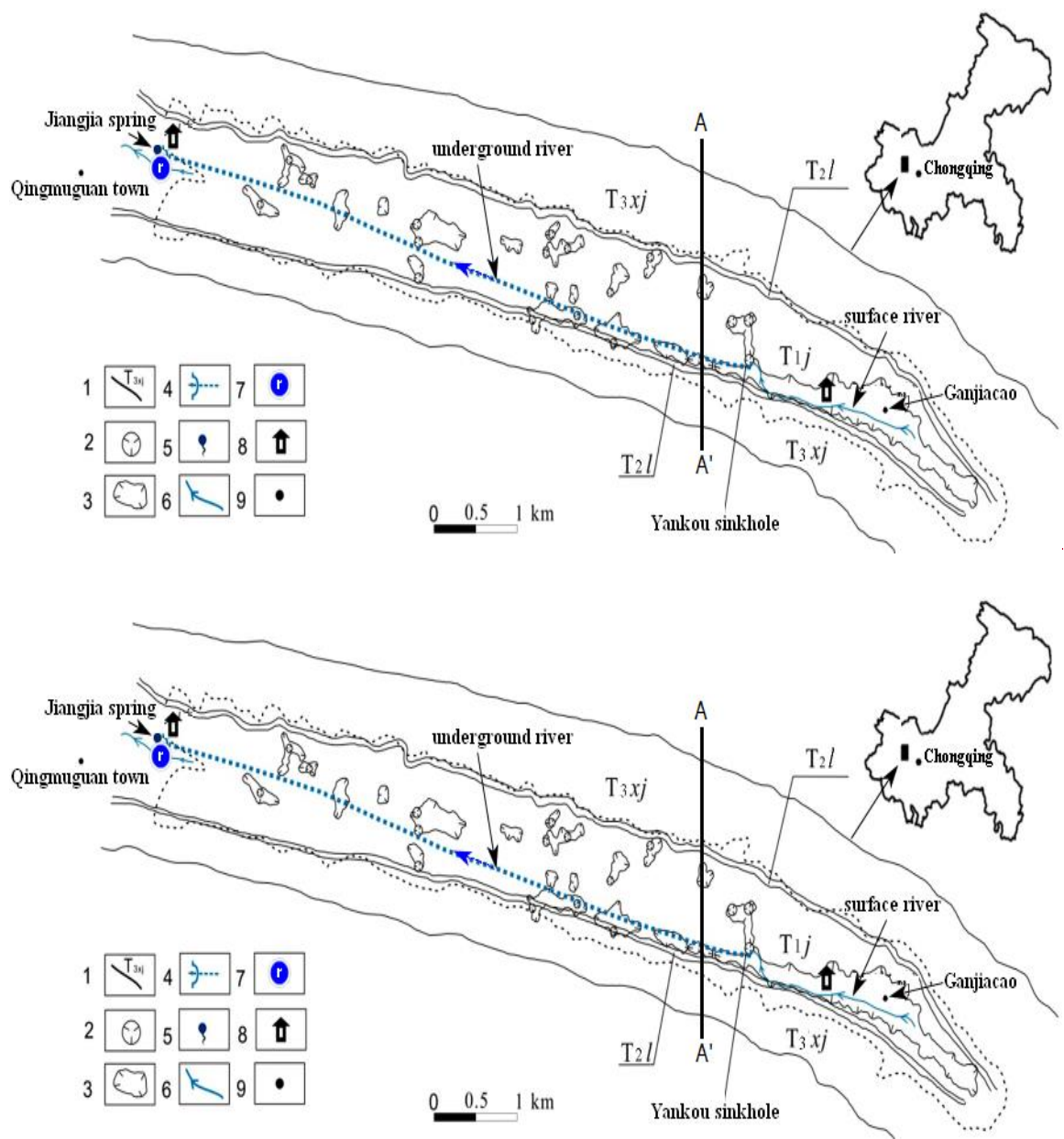
Parameter optimization	Parameter types	Nash coefficient	Correlation coefficient	Relative flow process error/%	Flood peak error/%	Water balance coefficient	Peak time error/(h)
calibration Calibration	initial Initial	0.82	0.77	24	29	0.82	-5
periods	optimized Optimized	0.91	0.94	14	12	0.95	-2
validation Validation	initial Initial	0.79	0.71	29	32	0.77	-4
periods	optimized Optimized	0.88	0.87	18	16	0.92	-2
average Average	initial Initial	0.81	0.74	27	31	0.8	-5
value	optimized Optimized	0.9	0.91	16	14	0.94	-2

Table 4 Flood simulation indices for model validation.

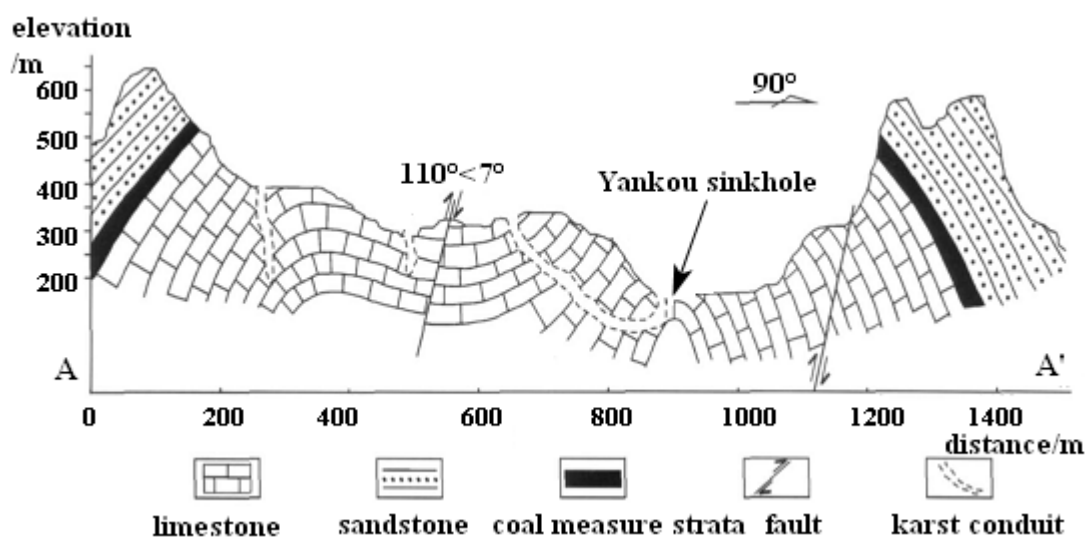
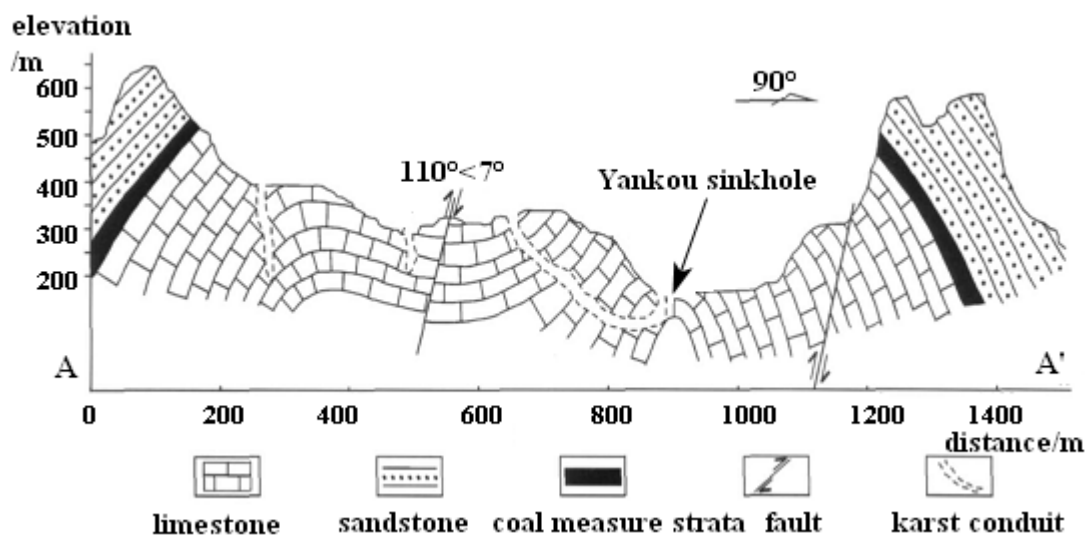
Floods	Parameter types	Nash coefficient	Correlation coefficient	Relative flow process error/%	Flood peak error/%	Water balance coefficient	Peak time error/(h)
2017042408	initial Initial	0.77	0.7	28	29	0.71	-5
	optimized Optimized	0.95	0.89	11	15	0.88	-2
2017050816	initial Initial	0.78	0.71	19	19	0.76	-4
	optimized Optimized	0.92	0.88	11	9	0.94	-2
2017061518	initial Initial	0.76	0.6	25	32	0.63	-5

	optimized <u>Optimized</u>	0.91	0.93	12	11	0.95	-3
	initial <u>Initial</u>	0.78	0.82	25	37	0.64	-4
2017071015-	optimized <u>Optimized</u>	0.92	0.87	8	7	0.94	-2
	initial <u>Initial</u>	0.81	0.62	21	16	0.78	-5
2017091512-	optimized <u>Optimized</u>	0.9	0.92	13	10	0.9	-4
	initial <u>Initial</u>	0.75	0.68	30	26	0.62	-2
2017100815-	optimized <u>Optimized</u>	0.94	0.86	11	15	0.92	-1
	initial <u>Initial</u>	0.78	0.68	25	21	0.67	5
2018052016-	optimized <u>Optimized</u>	0.91	0.93	10	13	0.94	2
	initial <u>Initial</u>	0.82	0.79	27	22	0.69	-6
2018060815-	optimized <u>Optimized</u>	0.9	0.92	11	12	0.93	-4
	initial <u>Initial</u>	0.84	0.75	26	24	0.61	5
2018071212-	optimized <u>Optimized</u>	0.91	0.88	8	15	0.92	3
	initial <u>Initial</u>	0.71	0.78	26	24	0.78	-4
2018081512-	optimized <u>Optimized</u>	0.89	0.94	12	11	0.89	-3
	initial <u>Initial</u>	0.85	0.68	28	23	0.68	-5
2018090516-	optimized <u>Optimized</u>	0.93	0.87	12	10	0.92	-2
	initial <u>Initial</u>	0.79	0.78	23	19	0.59	5
2018092514-	optimized <u>Optimized</u>	0.88	0.88	9	11	0.89	2
	initial <u>Initial</u>	0.78	0.81	28	25	0.63	5
2018101208-	optimized <u>Optimized</u>	0.92	0.94	11	10	0.94	2
	initial <u>Initial</u>	0.79	0.81	25	24	0.65	-6
2018111208-	optimized <u>Optimized</u>	0.94	0.86	13	12	0.92	-2
	initial <u>Initial</u>	0.78	0.8	26	36	0.8	5
2019042512-	optimized <u>Optimized</u>	0.89	0.94	9	16	0.93	2
	initial <u>Initial</u>	0.84	0.77	32	27	0.79	4
2019051513-	optimized <u>Optimized</u>	0.91	0.88	9	13	0.95	2
	initial <u>Initial</u>	0.74	0.75	29	26	0.63	-5
2019052516-	optimized <u>Optimized</u>	0.92	0.86	7	15	0.96	-2
	initial <u>Initial</u>	0.85	0.83	28	25	0.78	-4
2019060518-	optimized <u>Optimized</u>	0.95	0.96	10	12	0.92	-2
average <u>Average</u>	initial <u>Initial</u>	0.79	0.74	26	25	0.69	5
value	optimized <u>Optimized</u>	0.92	0.9	10	11	0.92	2

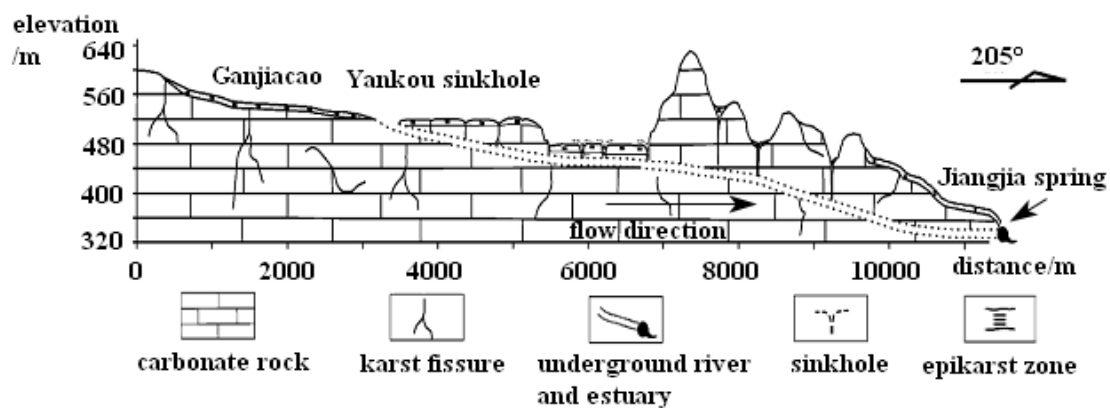
Figures

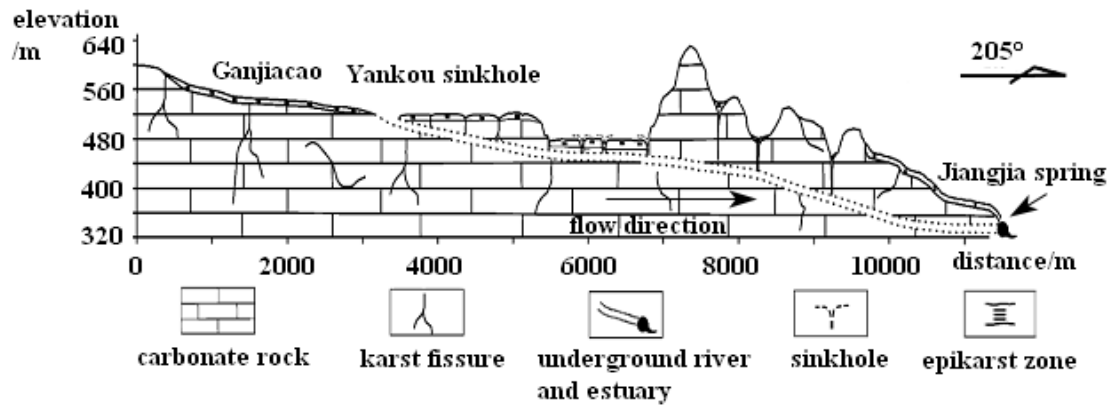


1- stratigraphic boundary, 2- sinkhole, 3- karst depression, 4- underground river, 5- karst spring, 6- surface river, 7- river gauge, 8- rain gauge, and 9- geographical name
a. Qingmuguan karst basin (modified from Yu et al., 2016)



b. Lithologic cross section AA' of the Yankou sinkhole/AA' (modified from Zhang, 2012)





c. Longitudinal profile of the study area (modified from Yang et al.,2008)

Figure 1 The Qingmuguan karst basin.

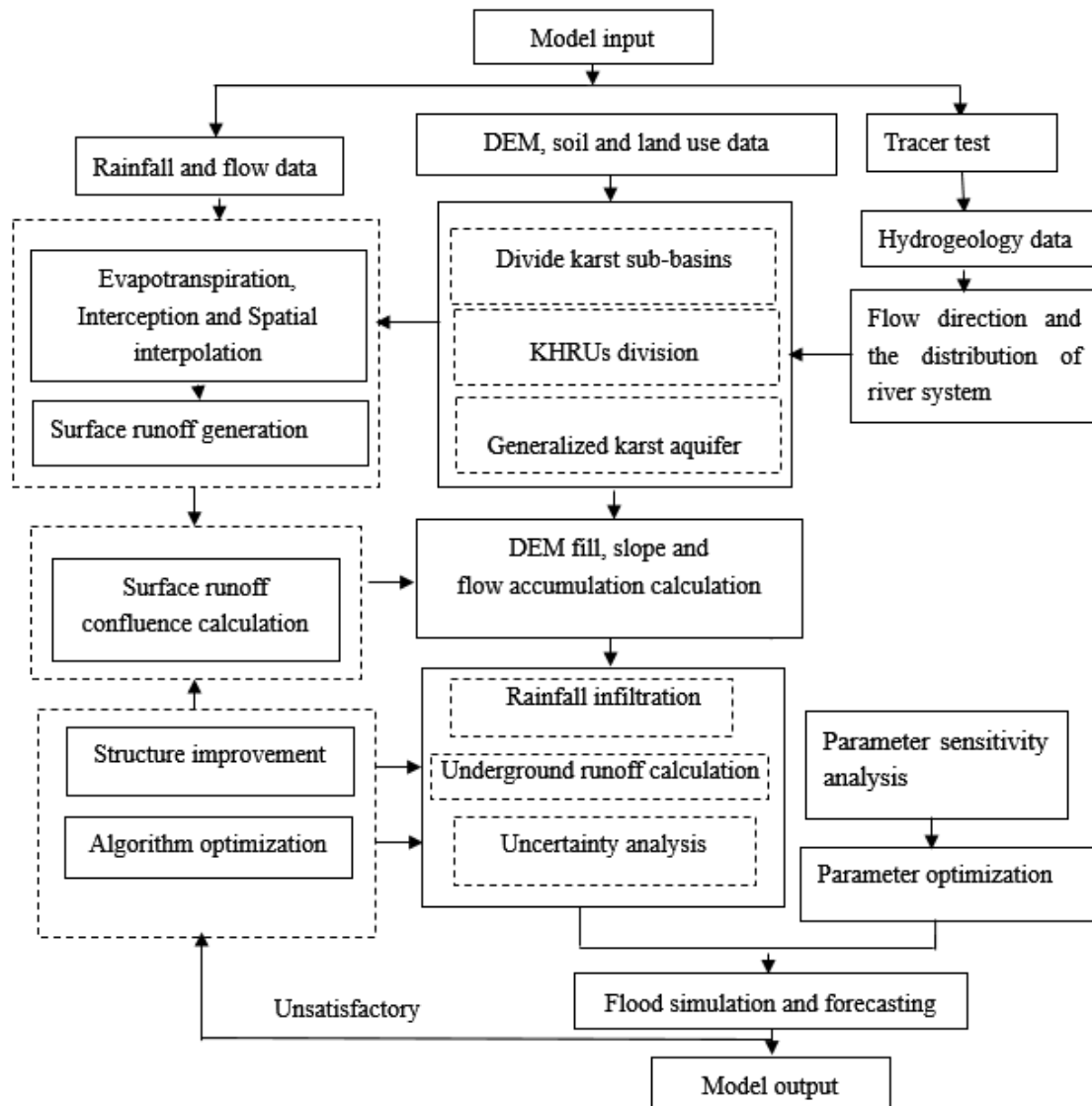


Figure 2 ~~Modeling flow chart~~Modelling flowchart of the QMG (Qingmuguan) model.

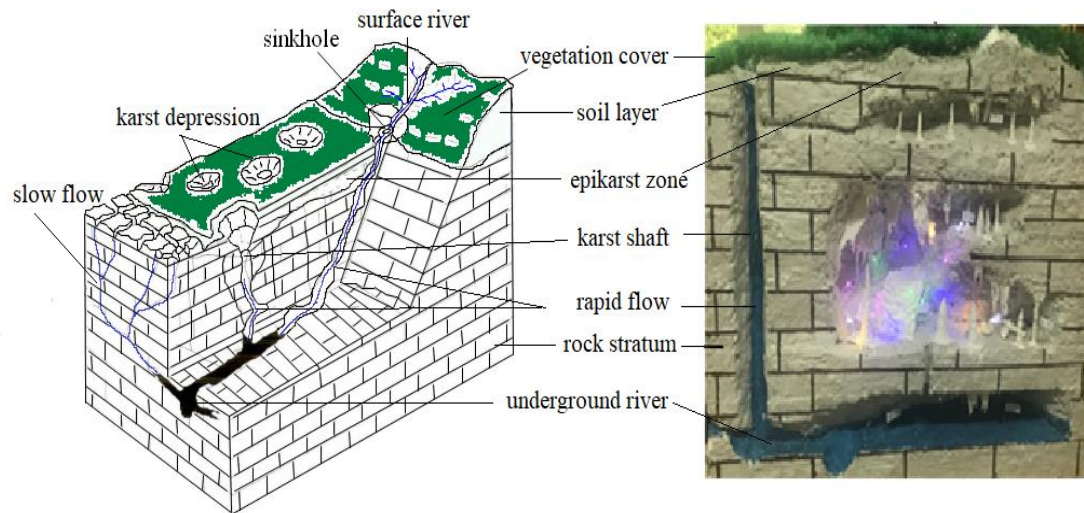
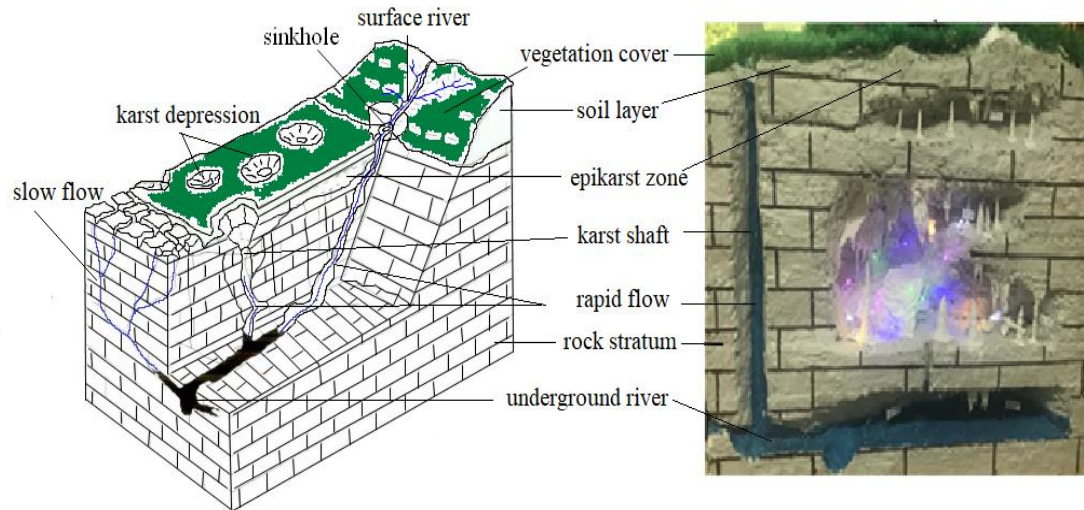
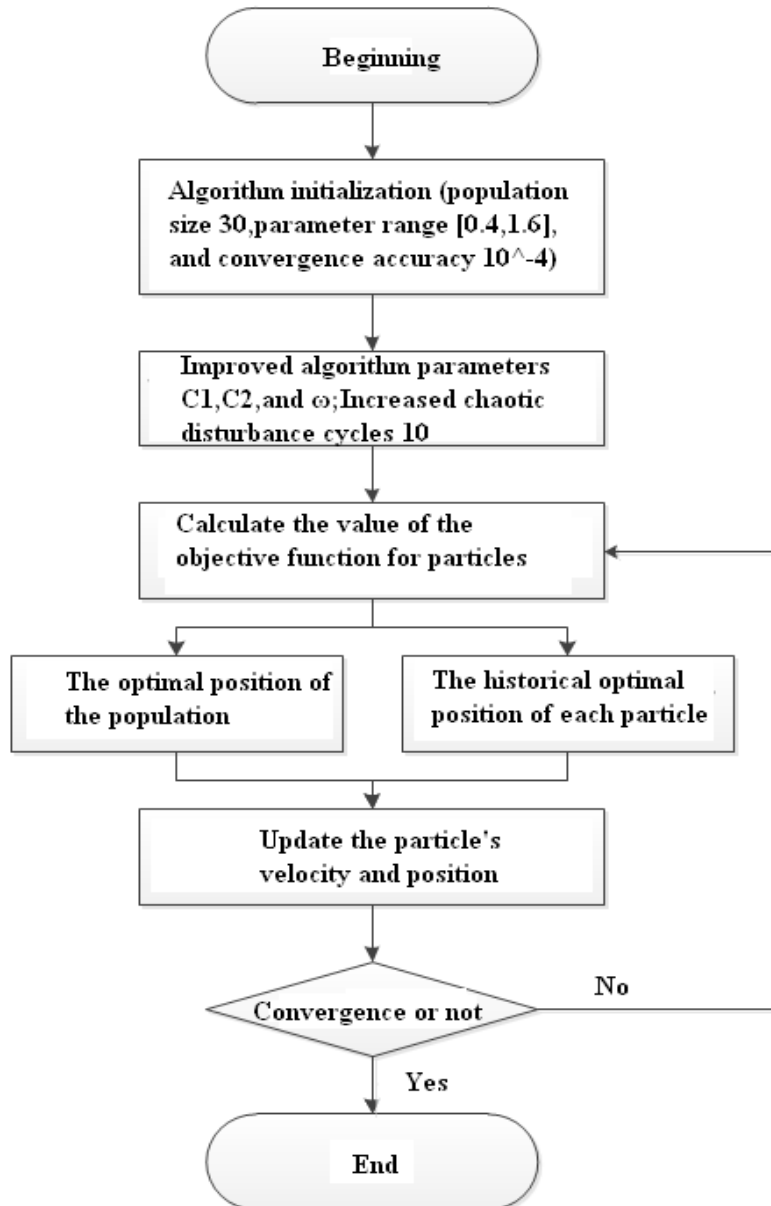
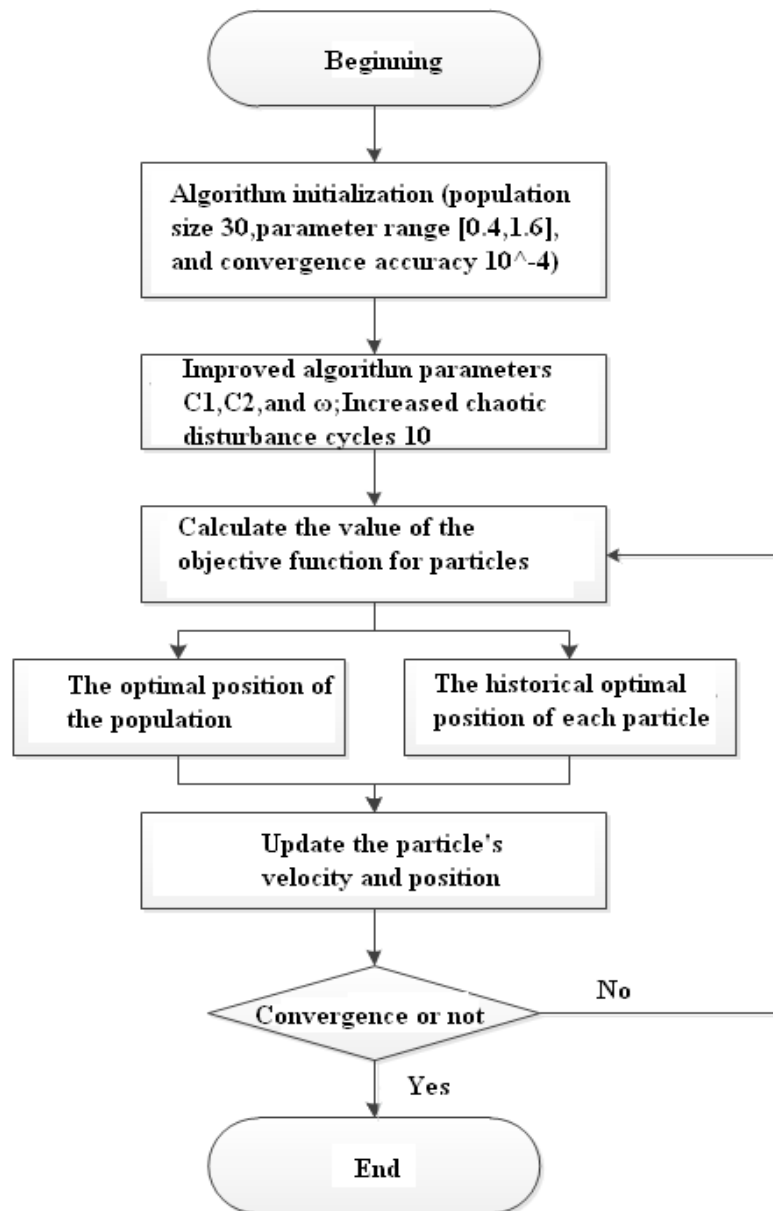


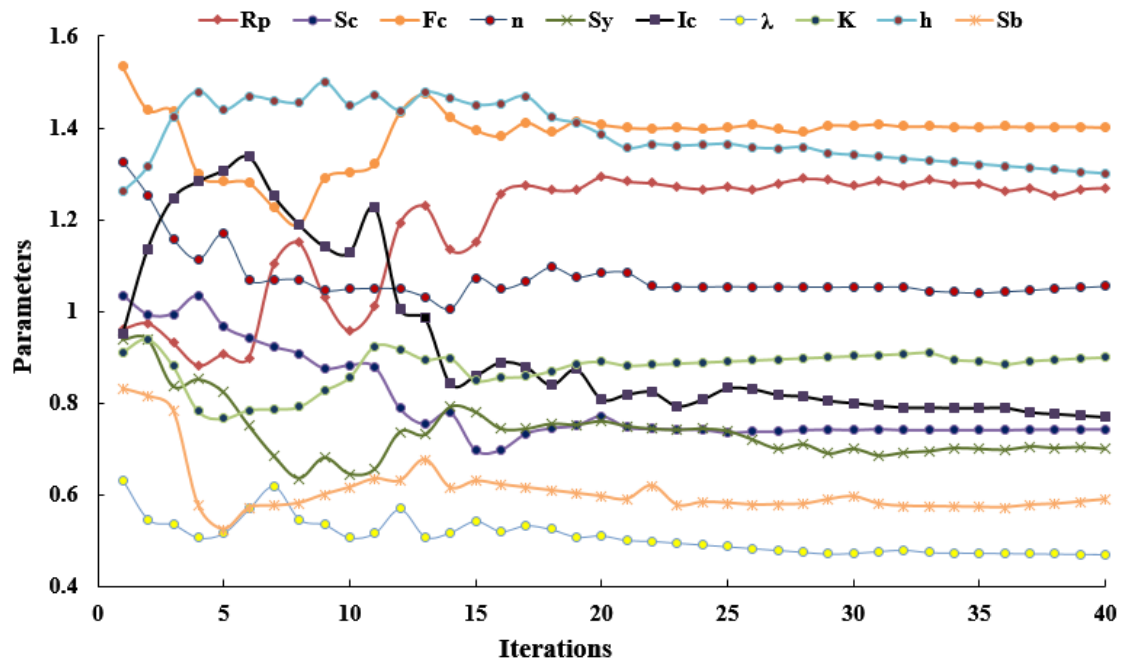
Figure 3 Spatial structure of the KHRUs (Li et al., 2021).-



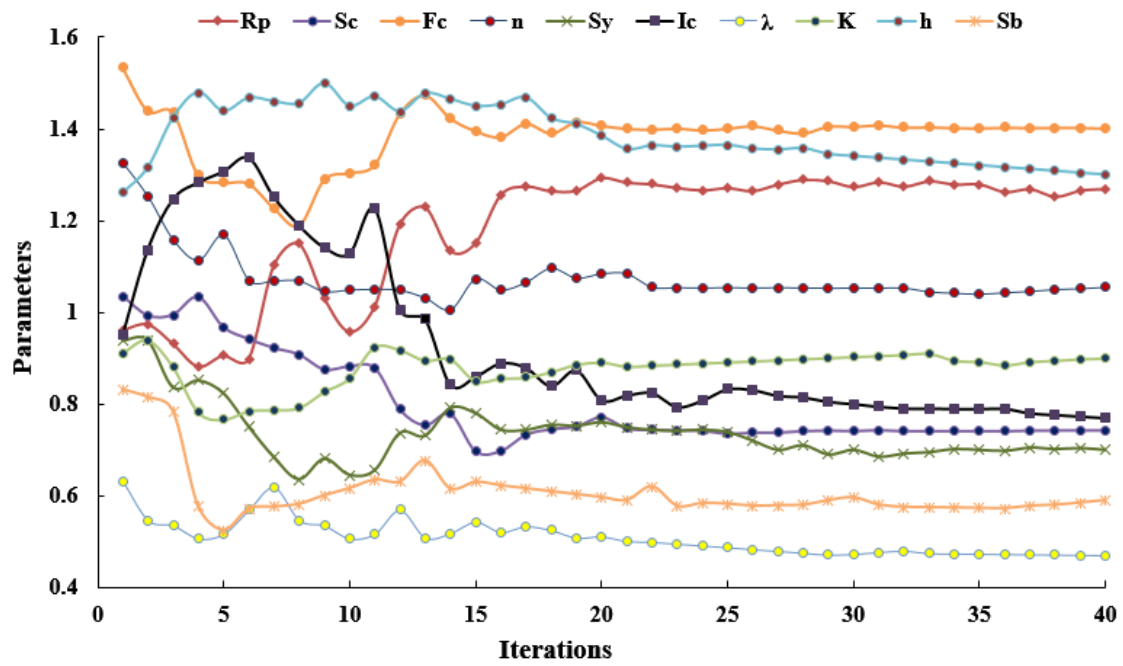


1096

Figure 4 Algorithm ~~flow-chart~~flowchart of the-IPSO.



1097



1098

1099

Figure 5 ~~Iteration~~Iterative process of ~~parametric~~parameter optimization.

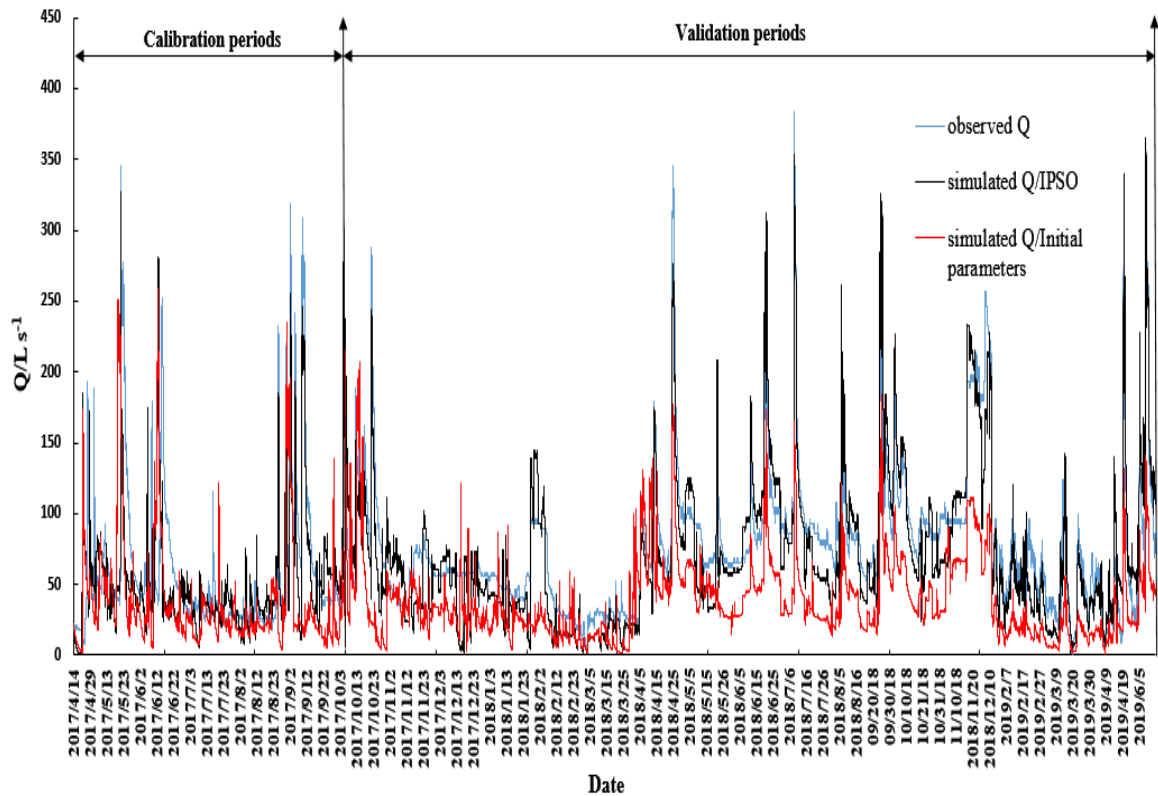
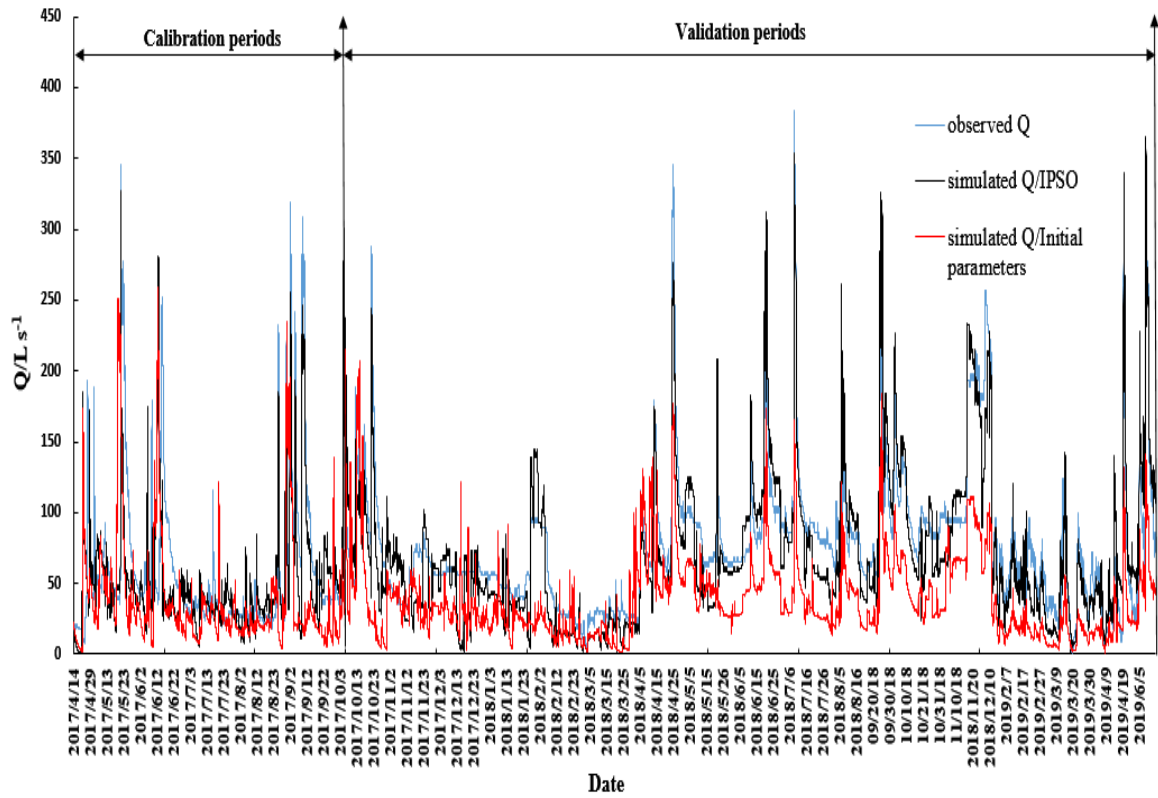
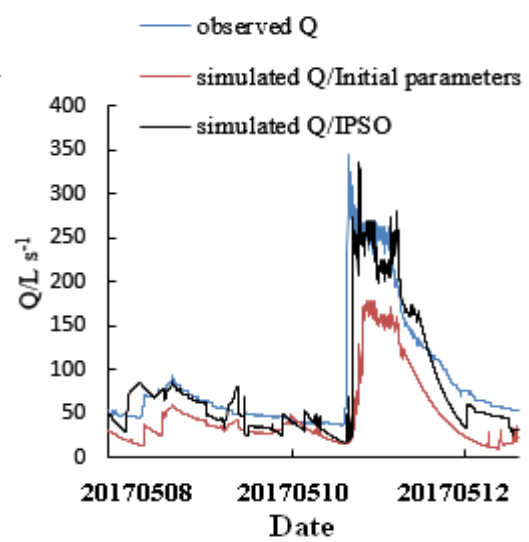
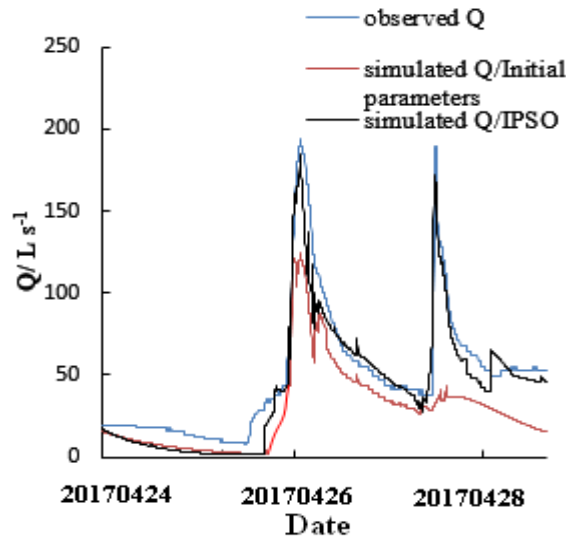
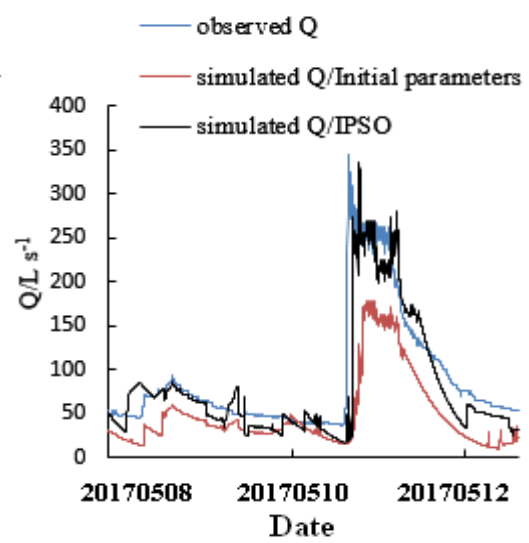
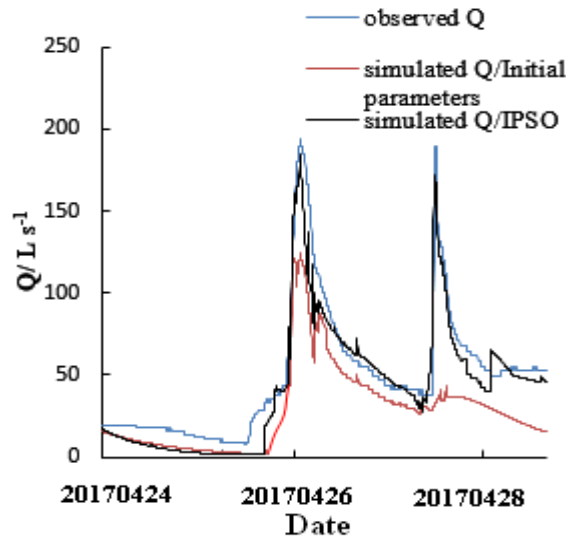
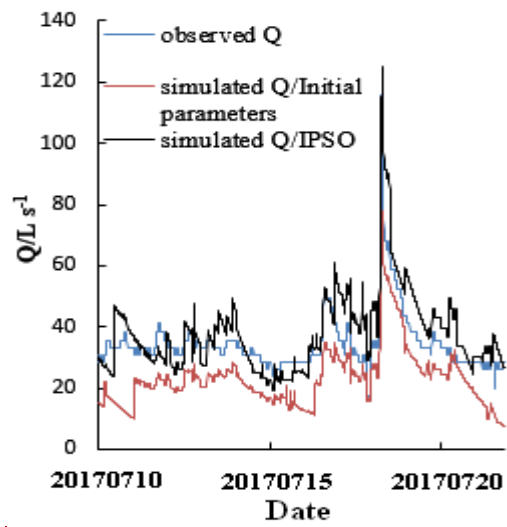
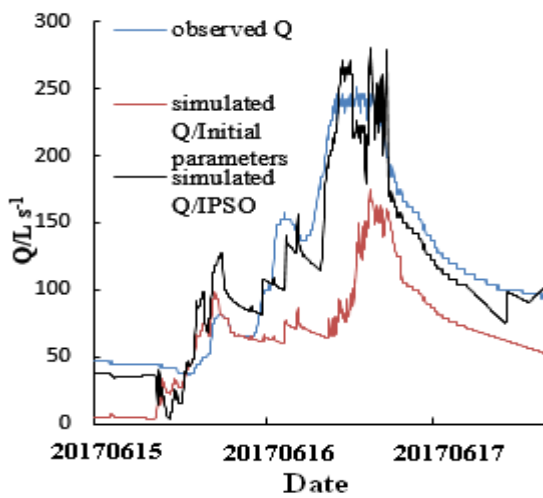


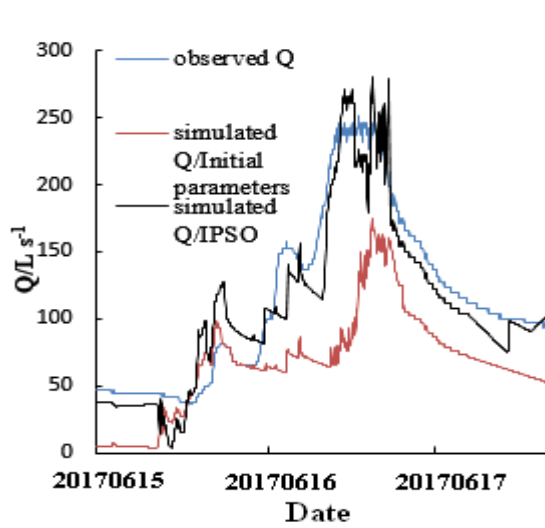
Figure 6 Flow simulation results of the QMG model based on parameter optimization.



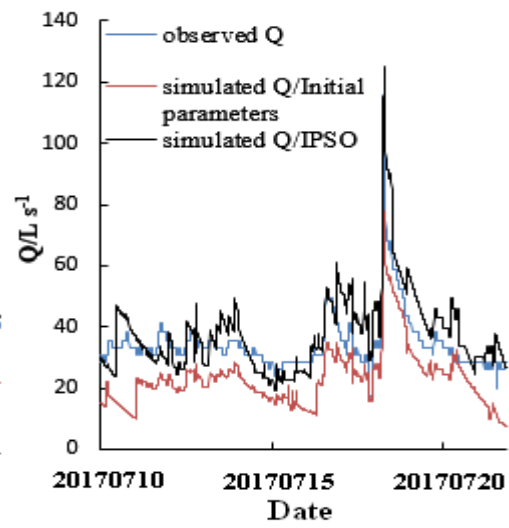
a. flood 201704240800

b. flood 201705081600

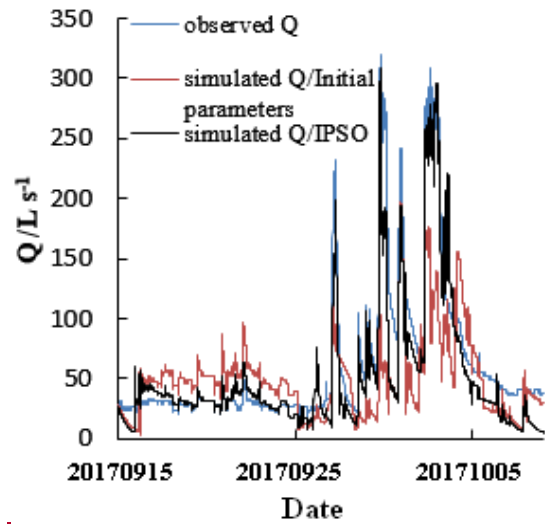




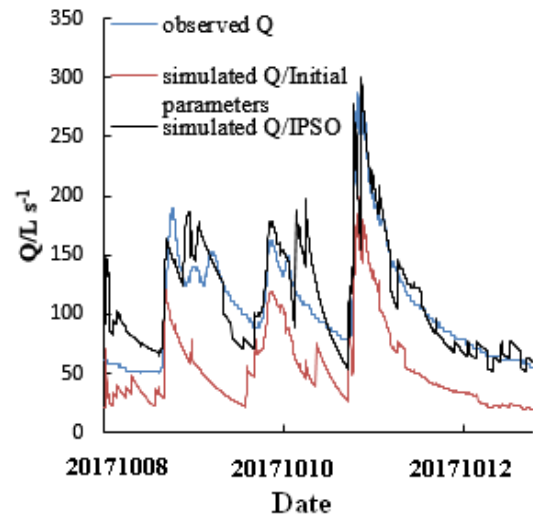
c. flood 201706151800



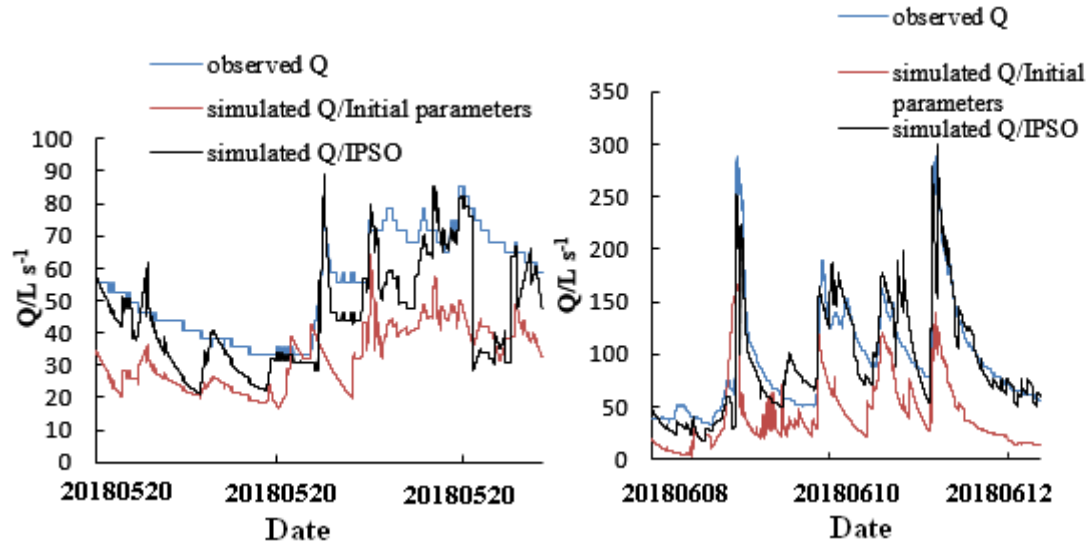
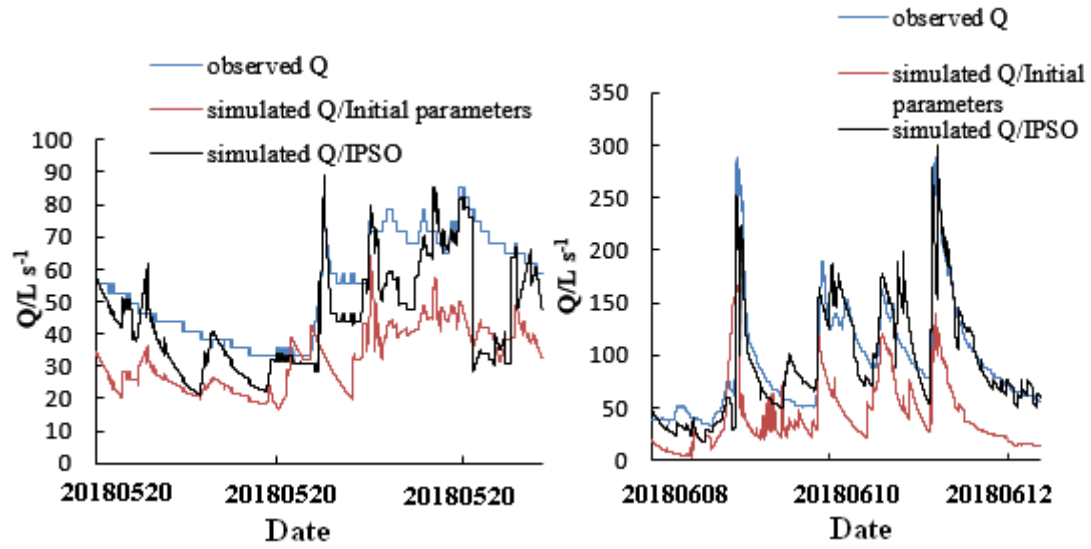
d. flood 201707101530



e. flood 201709151200

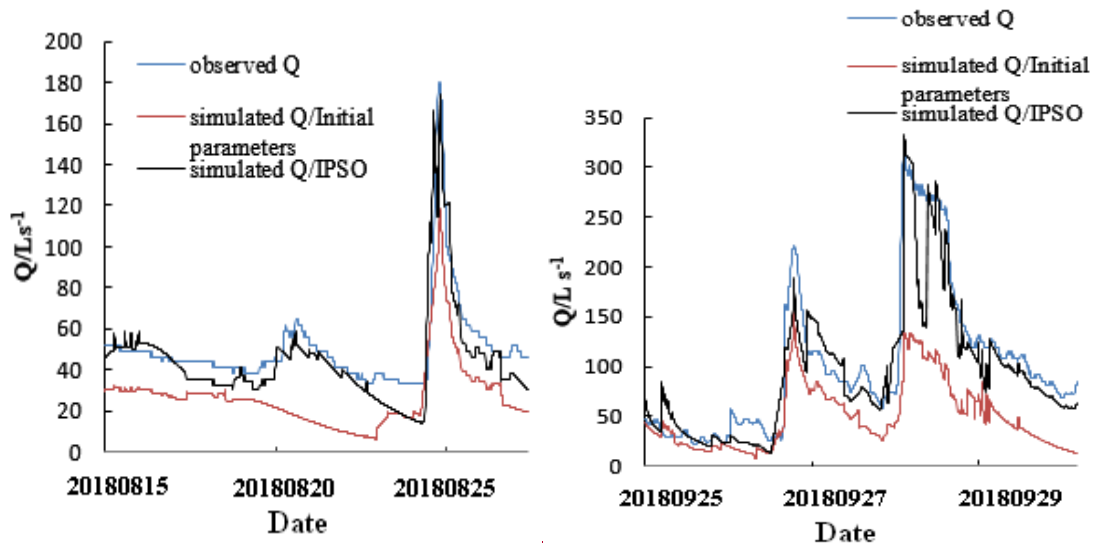


f. flood 201710081500



g. flood 201805201600

h. flood 201806081500



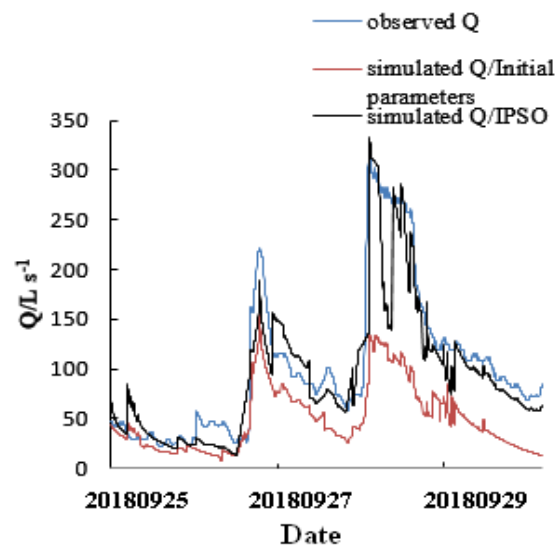
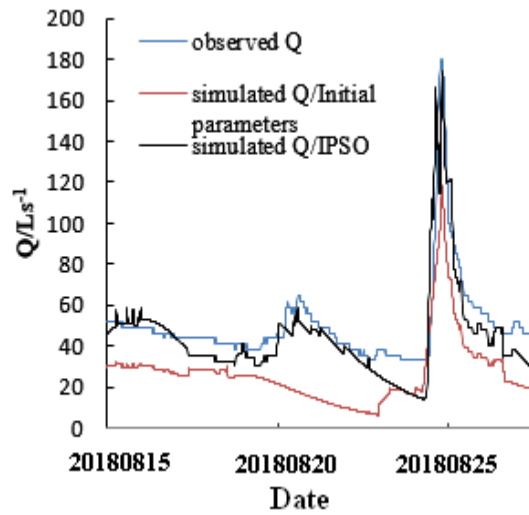


Figure 7 Flood simulation effects based on the initial and optimized parameters.